МІНІСТЕРСТВО ОСВІТИ І НАУКИ УКРАЇНИ
НАЦІОНАЛЬНИЙ АВІАЦІЙНИЙ УНІВЕРСИТЕТ
ФАКУЛЬТЕТ АЕРОНАВІГАЦІЇ, ЕЛЕКТРОНІКИ ТА ТЕЛЕКОМУНІКАЦІЙ
КАФЕДРА АЕРОКОСМІЧНИХ СИСТЕМ УПРАВЛІННЯ

ДОПУСТИТИ ДО ЗАХИСТУ
Завідувач кафедри
_____Юрій МЕЛЬНИК
«_____» _____2024 р.

КВАЛІФІКАЦІЙНА РОБОТА

(ПОЯСНЮВАЛЬНА ЗАПИСКА)

ВИПУСКНИКА ОСВІТНЬОГО СТУПЕНЯ
«БАКАЛАВР»

Тема: «**Оцінка компонентів зміщення нуля сучасних високоточних гіроскопів з використанням дисперсії Аллана**»

Виконавець: студент групи СУ-404 _____ Олексій ШАРАНДАК

Керівник: професор _____ Валерій ЧІКОВАНІ

Нормоконтролер: _____ Микола ДИВНИЧ

Київ 2024

MINISTRY OF EDUCATION AND SCIENCE OF UKRAINE
NATIONAL AVIATION UNIVERSITY
FACULTY OF AIR NAVIGATION, ELECTRONICS AND TELECOMMUNICATIONS
AEROSPACE CONTROL SYSTEMS DEPARTMENT

APPROVED FOR DEFENCE
Head of the Department
_____ Yurii MELNYK
“____” _____ 2024

QUALIFICATION PAPER

(EXPLANATORY NOTE)

FOR THE ACADEMIC DEGREE OF BACHELOR

Title: **“The estimation of the bias components of modern high-grade gyroscopes using the Allan variance**”

Submitted by: student of group CS-404 _____ Oleksii SHARANDAK

Supervisor: professor _____ Valerii CHIKOVANI

Standards inspector: _____ Mykola DYVNYCH

Kyiv 2024

НАЦІОНАЛЬНИЙ АВІАЦІЙНИЙ УНІВЕРСИТЕТ

Факультет аеронавігації, електроніки та телекомунікацій

Кафедра аерокосмічних систем управління

Спеціальність: 151 «Автоматизація та комп'ютерно-інтегровані технології»

ЗАТВЕРДЖУЮ

Завідувач кафедри

_____ Юрій МЕЛЬНИК

«_____»_____2024 р.

ЗАВДАННЯ

на виконання кваліфікаційної роботи

Шарандака Олексія Руслановича

1. Тема кваліфікаційної роботи «Оцінка компонентів зміщення нуля сучасних високоточних гіроскопів з використанням дисперсії Аллана» затверджена наказом ректора від «01» квітня 2024 р. № 511/ст.

2. Термін виконання роботи: з 13.05.2024 по 16.06.2024.

3. Вихідні дані роботи: Експериментальні дані багатогодинних випробувань гіроскопа з металевим резонатором середньої точності ТВГ-25 Українського виробництва та високоточного гіроскопа з кварцовим резонатором діаметром 20 мм Французького виробництва.

4. Зміст пояснювальної записки: Вступ, розділ 1-Сучасні високоточні гіроскопи, розділ 2 – Метод аналізу даних вимірів з використанням варіації Аллана, розділ 3 – Застосування методу варіації Аллана до високоточного гіроскопа, висновки, література.

5. Перелік обов’язкового ілюстративного матеріалу: Графіки результатів випробувань та графічне представлення кривих Аллана. Матеріали презентації в Power Point.

6. Календарний план-графік

№ пор.	Завдання	Термін виконання	Відмітка про виконання
1	Отримання теми дипломної роботи	13.05.2024	Виконано
2	Написання першого розділу роботи	17.05.2024	Виконано
3	Написання другого розділу роботи	27.05.2024	Виконано
4	Подача керівнику першого та другого розділів на перевірку	28.05.2024	Виконано
5	Написання третього розділу роботи	7.06.2024	Виконано
6	Подача керівнику третього розділу на перевірку	8.06.2024	Виконано
7	Оформлення дипломної роботи	12.06.2024	Виконано
8	Підготовка презентації доповіді	16.06.2024	Виконано

7. Дата видачі завдання: «13» травня 2024 р.

Керівник кваліфікаційної роботи _____ Валерій ЧІКОВАНІ
(підпис керівника)

Завдання прийняв до виконання _____ Олексій ШАРАНДАК
(підпис випускника)

NATIONAL AVIATION UNIVERSITY

Faculty of Air Navigation, Electronics and Telecommunications

Aerospace Control Systems Department

Specialty: 151 “Automation and Computer-integrated Technologies”

APPROVED BY

Head of the Department

_____ Yurii MELNYK

“_____”_____2024

Qualification Paper Assignment for Graduate Student

Sharandak Oleksii Ruslanovych

1. The qualification paper title “The estimation of the bias components of modern high-grade gyroscopes using the Allan variance” was approved by the Rector’s order of “ 01 ” April 2024 № 511/ст.

2. The paper to be completed between: 13.05.2024 and 16.06.2024

3. Initial data for the paper: Experimental data of long-term tests of a gyroscope with a medium-precision metal resonator TVG-25 of Ukrainian production and a high-precision gyroscope with a quartz resonator with a diameter of 20 mm of French production.

4. The content of the explanatory note: Introduction, Section 1 - Modern High Precision Gyroscopes, Section 2 - Allan's Variation Method for Measurement Data Analysis, Section 3 - Application of Allan's Variation Method to a High Precision Gyroscope, Conclusion, References.

5. The list of mandatory illustrations: Graphs of test results and graphical presentation of Allan curves. Presentation materials in Power Point

6. Timetable

№	Assignment	Dates of completion	Completion mark
1	Obtaining a thesis topic	13.05.2024	Done
2	Writing the first chapter of the work	17.05.2024	Done
3	Writing the second chapter of the work	27.05.2024	Done
4	Submitting the first and second sections to the manager for review	28.05.2024	Done
5	Writing the third chapter of the work	7.06.2024	Done
6	Submission to the head of the third section for review	8.06.2024	Done
7	Completion of the thesis	12.06.2024	Done
8	Preparation of the presentation of the report	16.06.2024	Done

7. Assignment issue date: “13” May 2024

Qualification paper supervisor _____ Valerii CHIKOVANI
(the supervisor’s signature)

Issued task accepted _____ Oleksii SHARANDAK
(the graduate student’s signature)

РЕФЕРАТ

Пояснювальна записка до дипломної роботи "Оцінка компонентів зміщення нуля сучасних високоточних гіроскопів з використанням дисперсії Аллана" містить 77 сторінок, 45 ілюстрацій, 32 джерела.

Актуальність теми полягає в необхідності точного визначення складових зміщення нуля сучасних високоякісних гіроскопів для визначення їхньої точності та напрямків їх застосування, таких як навігаційні системи, космічні та авіаційні технології, а також побудування моделей похибок для їх корегування.

Об'єктом дослідження є високоякісний вібраційний гіроскоп з кварцовими резонаторами в інерціальному вимірювальному блоці виробництва компанії Safran (Франція), а також одновісний гіроскоп ТВГ-25 виробництва компанії АТ «Елміз» (Україна)

Предметом дослідження є метод варіаційного аналізу Аллана для високоякісного вібраційного гіроскопа з кварцовим резонатором діаметром 20 мм.

Метою роботи є вивчання методів аналізу стохастичних похибок гіроскопів з використанням методу варіації Аллана для визначення напрямків їх застосування та побудування моделей похибок з метою їх корегування для підвищення точності.

Методи дослідження Розробка комп’ютерних програм для розрахунків параметрів, графічне визначення компонентів похибок, аналітичний аналіз методу варіації Аллана.

Ключові слова: КІЛЬЦЕВІ ЛАЗЕРНІ ГІРОСКОПИ, ВОЛОКОННО-ОПТИЧНІ ГІРОСКОПИ, ВІБРАЦІЙНІ ГІРОСКОПИ З КВАРЦОВИМ РЕЗОНАТОРОМ, ВАРІАЦІЙНИЙ АНАЛІЗ АЛЛАНА, ПАРАМЕТРИ ПОХИБОК.

ABSTRACT

Explanatory note for the qualification paper "The estimation of the bias components of modern high-grade gyroscopes using the Allan variance" includes: 77 pages, 45 illustrations, 32 sources.

The relevance of the topic is the need to accurately determine the components of the gyro bias of modern high-quality gyroscopes in order to determine their accuracy and directions of application, such as navigation systems, space, and aviation technologies, as well as to build error models for their correction

The object of the study is a high-quality vibrating gyroscope with quartz resonators in an inertial measuring unit manufactured by the Safran company (France), as well as a single-axis gyroscope TVG-25 manufactured by the JSC "Elmiz" company (Ukraine)

The subject of the research is Allan's method of variation analysis for a high-quality vibrating gyroscope with a 20 mm diameter quartz resonator.

The aim of the work is the study of the stochastic error analysis method of gyroscopes using the Allan variation method to determine the directions of their application and the construction of error models in order to correct them for increasing accuracy

Research methods are the development of computer programs for parameter calculations, graphical determination of error components, and analytical analysis of the Allan variation method.

Key words: MODERN HIGH-QUALITY GYROSCOPES, RING LASER GYROSCOPES, FIBER-OPTIC GYROSCOPES, VIBRATION GYROSCOPES WITH A QUARTZ RESONATOR, ALLAN VARIATIONAL ANALYSIS, ERROR PARAMETERS.

CONTENT

INTRODUCTION

Modern high-precision gyroscopes are essential components in various technical systems that require high stability and measurement accuracy. They are extensively utilized in contemporary aviation systems, space research, robotics, and other high-tech industries. The accuracy in determining the zero offset components is a critical measure of their efficiency and dictates their applicability in critical environments where navigation and orientation accuracy is paramount. Therefore, investigating these components and developing methods for their evaluation is a pressing scientific and technical challenge with significant practical potential for advancing control and navigation technologies.

Scientific and technical issues related to the evaluation of the zero offset components of high-precision gyroscopes are addressed across a broad spectrum of applications, including navigation systems, aviation technologies, space research, and industrial applications. The current state of research in this field underscores the importance of gyroscope accuracy and reliability for modern technologies and scientific advancements.

The primary foundational data for developing this topic includes an understanding of the principles of high-precision gyroscopes, methods for estimating their parameters, and knowledge of the Allan variance method and its application to gyroscope analysis.

The necessity for this study lies in enhancing the accuracy and reliability of high-precision gyroscopes, which are pivotal components in numerous modern control and navigation systems. Evaluating the zero offset components will enable the identification and correction of deviations that occur under real operating conditions.

Research on the evaluation of zero offset components has already yielded some practical results, highlighting an active interest in this issue and the potential for using the obtained data to improve technical systems.

At the world level, there is a constant development of methods for evaluating and correcting the zero offset components of gyroscopes. This indicates the relevance of the topic and the need to constantly update knowledge in this area.

The aim of this work is to evaluate the components of the high-precision gyroscopes bias using the Allan variance method, as well as to determine their impact on the accuracy and reliability of control systems. The feasibility study is to identify opportunities to apply the results obtained to improve the efficiency of technical systems and reduce the cost of their operation.

SECTION 1
MODERN HIGH-GRADE GYROSCOPES

1.1. Definition on gyroscope

Gyroscopes are important devices in aerospace technology that play an important role in ensuring stability and safety. These devices measure and maintain the orientation of an object in space or during flight. They are utilized in spacecraft, rockets, satellites, as well as in aircraft and helicopters. Their importance stems from their ability to help pilots and astronauts maintain necessary stability and control the movement of objects in space.

A gyroscope, whether mechanical or electronic, operates on the principle of angular momentum to maintain its alignment relative to the Earth's axis or to resist changes in its alignment. Typically, a gyroscope consists of a rotating rotor that generates angular momentum and a series of gimbals or pivot supports.

Each gyroscope is centered around one or more axes, which are fundamental to its structure. The rotation axis is often aligned with the Z-axis, allowing the gyroscopic rotor to rotate freely, which is crucial for its functionality. The housing or framework, along with bearings, provides structural integrity and protects the internal mechanisms.

While single-axis gyroscopes operate around a single rotational axis, others, such as three-axis gyroscopes, are designed to detect motion and changes in orientation across all three spatial axes: X, Y, and Z. The specific number and arrangement of these axes can vary depending on the gyroscope's design and intended use.

Conceptually, a single-axis gyroscope resembles a seesaw that oscillates in one direction only, measuring or responding to motion along that axis. Conversely, a three-axis gyroscope behaves akin to a spinning top that can be manipulated in various directions: forward and backward (X-axis), side to side (Y-axis), and even in a rotational manner like a top (Z-axis) [1].

1.2. Gyroscopic Stability

Gyroscopes essentially replicate the Earth's stability in its rotation, enabling engineers and scientists to achieve precise and stable motion or orientation in various applications, from navigation systems to spacecraft [2].

In the rapidly evolving field of aerospace engineering, accurate measurement is the cornerstone of technological progress. The effectiveness of gyroscopic instruments depends on their ability to precisely measure angular velocity. Advanced technologies such as Ring Laser Gyros (RLG), Fiber-Optic Gyros (FOG), and Vibratory Gyros with Quartz Resonators (HRG) utilize the Sagnac effect, light interference in optical fibers, and mechanical vibrations of quartz resonators, respectively. These sophisticated technologies, which merge principles of physics and engineering, provide a detailed understanding of motion essential for today's advanced aerospace sector.

RLGs, FOGs, and HRGs are prime examples of technological excellence in aerospace engineering, a field led by industry giants like Honeywell, KVH Industries, and Safran. These gyroscopic systems are designed to meet the complex challenges of aviation dynamics, demonstrating the industry's dedication to innovation and precision.

Integrating gyroscopes into Inertial Measurement Units (IMUs) is a critical aspect of aerospace navigation. IMUs combine data from gyroscopes and accelerometers, playing a vital role in ensuring precise navigation in aircraft. This

integration is crucial for accurate inertial measurements, essential for maintaining spatial orientation and accuracy during flight.

Evaluating gyroscopic performance metrics, such as accuracy, bias stability, and drift resistance, is of utmost importance in the aerospace sector. Thorough testing and validation of these parameters ensure the reliability and effectiveness of gyroscopic systems in the demanding and variable conditions of aerospace missions.

This study not only explores the technological aspects but also delves into scientific investigation at the forefront of precision measurement in aviation. The development of advanced gyroscopic technologies highlights not just technological progress but also the ongoing interaction between scientific research and practical applications vital for advancements in aerospace engineering.

As we proceed with this exploration, each section will detail the complexities of these gyroscopic technologies, laying a solid foundation for the subsequent analysis of the Allan variance estimation methodology within the aviation context.

1.3.1. Introduction to Ring Laser Gyros (RLG) in Aerospace Applications

Ring Laser Gyroscopes (RLGs) represent the pinnacle of gyroscopic technology, especially in the aerospace industry. This chapter is dedicated to an in-depth examination of RLGs, detailing their manufacturing intricacies, applications in inertial measurement instruments (IMIs), and critical performance parameters.

Gyroscopes are devices used to measure and maintain the orientation of an object in inertial space at any given time. Prior to the advent of RLG technology, mechanical gyroscopes were the standard.

RLGs have a significant advantage over traditional mechanical gyroscopes due to their lack of moving parts, which considerably reduces wear and tear, thereby enhancing their reliability and lifespan. They are also immune to many of the errors that affect mechanical gyroscopes, such as friction and imbalance. Furthermore,

RLGs offer high precision and accuracy, making them indispensable in applications where exact orientation and navigation data are crucial, such as in spacecraft, aircraft, submarines, and some ground-based vehicles. Their robustness and ability to provide precise measurements under varying conditions make them essential components of modern inertial measurement units (IMUs), which are critical for the guidance, navigation, and control of many high-tech systems.

RLGs are the industrial standard today and utilize the Sagnac effect for orientation determination, manifested in a ring interferometer. An interferometer is where the ring laser gyroscope is initially configured. Interferometers are instruments used in research that operate by combining two or more light sources to produce an interference pattern, which is subsequently observed and analyzed. They are frequently employed for extremely precise measurements that are not feasible using alternative methods, such as discerning alterations in microscopic entities or identifying gravitational waves. Interferometers find application across a broad spectrum of fields due to their sensitivity and versatility.

The interferometer used for a ring laser gyroscope comprises narrow tunnels that form a closed loop around a block of zero-expansion glass made from lithium, aluminum, and silicon oxides. To create the interference pattern for the Sagnac effect, three mirrors are placed at each vertex, and two laser beams propagating in opposite directions are formed in the active cavity.

Although the beams travel in opposite directions, they enter and exit at the same point, allowing the interferometer to measure the collected signal at the moment of exit. As the ring laser gyroscope moves, the light beams travel different distances. The difference in frequency is proportional to the speed of rotation. The frequency difference is measured using an interference pattern whose phase contains information about direction [3]. The principle of operation of the laser gyroscope can be seen in the image demonstrating the basic operation of the ring laser gyroscope (Fig. 1.3.1, Fig. 1.3.2).

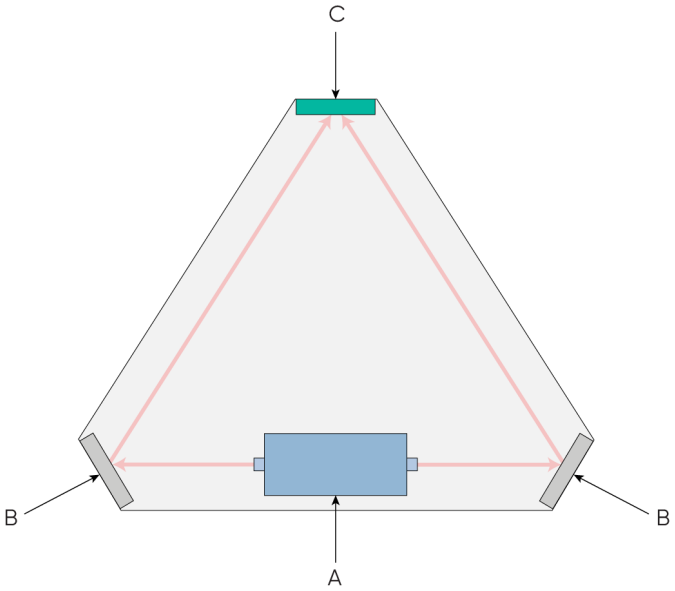

Fig. 1.3.1. How it works: The laser source (A) emits beams of light simultaneously in opposite directions; The laser source (A) emits beams of light simultaneously in opposite directions. The light is reflected by mirrors (B), which direct it to an optical receiver (C)

Any rotation of the device causes the light rays to reach the optical receiver at different times due to the Sagnac effect, which can be extrapolated to rotation measurements [4].

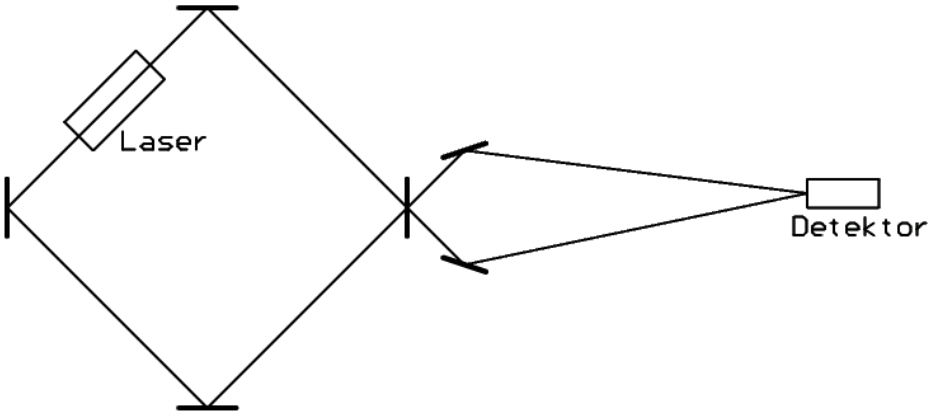

Fig. 1.3.2. Scheme of a laser gyroscope

Here, the laser beam is circulated by means of mirrors and continuously amplified by a laser (or rather a quantum amplifier). The closed loop has a branch

through a translucent mirror (or, for example, through a slit) to an interferometer-based sensor [5].

Laser gyroscopes offer several advantages over electromechanical ones, leading to a broad range of practical applications. For system control designers, the extraction method and form of output data from gyroscopes are critical.

A laser gyroscope provides highly convenient control signals at its output, such as a sequence of electrical pulses, with polarity determined by the gyroscope's rotation direction. The number of individual pulses, such as 16, is proportionate to small fixed increments of rotation angle (e.g., one second of arc). The total rotation angle of the gyroscope is calculated based on the total number of pulses. Precision in operation is even more critical for designers.

The precision of laser gyroscopes is exceptionally high. They are designed to detect rotation speeds of less than 0.1 degrees per hour, requiring the measurement of differences in optical trajectories with an accuracy of 10^-5 nanometers and frequency changes of about 0.1 Hz (at operational frequencies of 10^14-10^15 Hz) [6].

Let's consider photos of different laser gyroscopes.

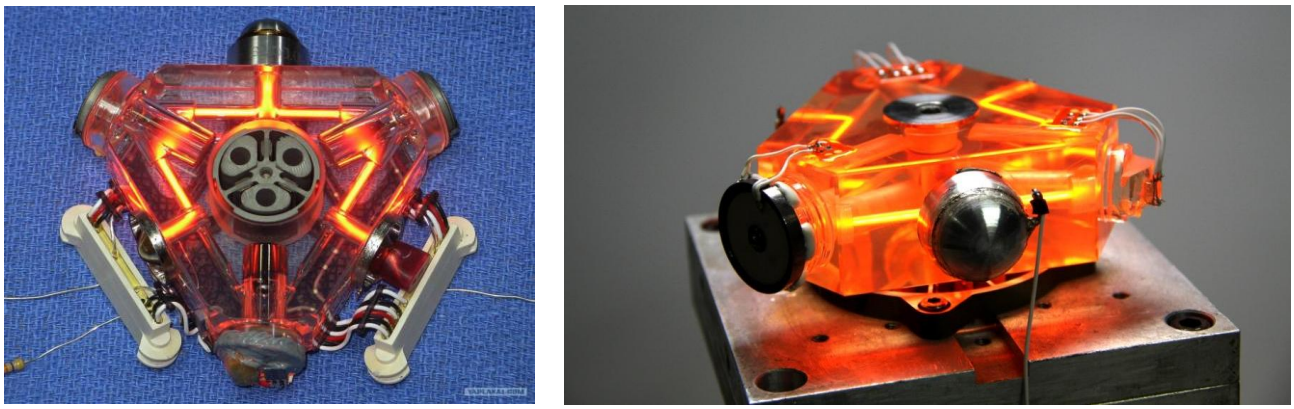

Fig. 1.3.3. Three-mirror RLG

Fig. 1.3.4. Four-mirror RLG

1.3.2. Inertial Measurement Unit (IMUs) based on RLG

RLGs serve as the basis for building high-performance inertial measurement units (IMUs). These IMUs, which are an integral part of aerospace navigation, combine RLG measurements with accelerometers to provide a comprehensive understanding of aircraft movement in three dimensions.

Here are some examples of inertial measurement devices based on a laser ring gyroscope:

1. Gyrolaser: A gyrolaser is a special type of laser ring gyroscope used to measure orientation and rotation in spacecraft. It uses laser technology to achieve high measurement accuracy and stability.

2. INS (Inertial Navigation System): Inertial navigation systems used in aviation and maritime transport to determine the position, speed and orientation of an object in space. These systems include a set of inertial measuring devices such as laser ring gyroscopes, accelerometers and magnetometers.

3. AR/VR Headsets: Some AR/VR devices are configured with built-in inertial measurement devices based on laser ring gyroscopes to measure the orientation of the

user's head. This allows for accurate reproduction of head rotation and displacement to create an explicit 3D space.

4. Autonomous cars: Some autonomous vehicles choose inertial measurement devices based on laser ring gyroscopes to measure, position the rotation and orientation of the vehicle. This will confidently determine the position and motion of the vehicle simultaneously without using external sensors. These are just a few examples of applications for laser ring gyroscope-based inertial measurement devices. This technology is used in many industries where it is necessary to accurately measure the angular velocity and orientation of objects.

Example of RLG-based IMU is MH-JG132A Three-axis Monolithic Ring Laser Gyroscope (Fig. 1.3.5). The first three-axis monolithic ring laser gyroscope, the JG132A, was developed as a three-axis monolithic ring laser gyroscope (MRLG) with two laser gyroscope assemblies and a single-axis laser gyroscope. The accelerometer mounting location can be reserved according to user needs. The JG132A is equipped with a special dedicated secondary power supply.

The main function of the accelerometer is to accurately measure information about the angular vector of motion relative to inertial space, which can be displayed to the user in the form of angular increments. The JG132A is used in system developments such as inertial navigation, positioning and orientation, and position determination.

Fig. 1.3.6. Inertial Measurement Unit Based on Four-mirror RLG With Dithers

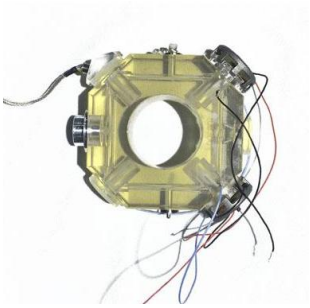

Fig. 1.3.7. JG132 Three-axis monolithic ring laser gyroscope

JG132A (Fig. 1.3.7) three-axis Monolithic Ring Laser Gyroscope has been successfully utilized in vehicle navigation systems, strap-down inertial navigation systems, mobile position and attitude determination systems. Table 1 shows the characteristics of this IMU.

Table 1

Characteristics of JG132A three-axis Monolithic Ring Laser Gyroscope

NO.	ITEM	INDEX		NOTES
		Class A	Class B	
1	Roll, Pitch and Azimuth Angular Rate	≦±300°/S		
2	Constant Bias	≦±0.5°/h	≦±0.5°/h	
3	Bias Stability	≦0.015°/h	≦0.020°/h	1σ
4	Bias Repeatability	≦0.015°/h	≦0.020°/h	1σ
5	Output Angle Increment	≦0.58"/LSB		
6	Start-up Time	﹤20s		
7	Operating Temperature	-40°C～70°C		
8	Impact Force	15g/30g		
9	Dimensions	203m mXX195 mmXX130mm		
10	Weight	≦8kg		
11	Power	±5V, +12v, ±45V, -12v1, -12v2, -12v3, -12v4		
12	Data Communication	RS422		
13	Data Refresh Rate	100Hz		
14	Baud Rate	115200bps		

Operational parameters: The operational parameters of radars are critical metrics that determine their performance in real-world environments. Parameters such as bias stability, accuracy and robustness are key to assessing radar performance in the harsh environments encountered in aerospace operations.

Manufacturing excellence: Manufactured by industry leaders such as Honeywell, radars are an example of precision engineering. These instruments use the principles of the Sagnac effect to create a closed loop of laser beams, which provides exceptional angular velocity measurement accuracy. Understanding the manufacturing processes is fundamental to understanding the reliability and accuracy inherent in RLGs. Table 2 represent the RLG manufacturers and features [7].

Table 2

World leading RLG manufacturers and RLG main parameters.

Company	LG type and resonator geometry	Perimeter (cm.)	Bias repeatability, 3σ, (deg/h)	Bias instability, σ,(deg/h)	Random walk, 3σ, (deg/h$^{1/2}$)
Honeywell (США)	GG-1342 square	32	0.01	0.0005	0.002
Honeywell (США)	GG-1328 square	21.5	0.03-0.2	0.07	0.01
Honeywell (США)	GG-1320 square	17	0.006-0.03	-	0.003-0.01
Honeywell (США)	GG-1308 square	6.1	1.0	1.0	0.1
Litton (США)	LG-142 square	28	0.01	0.01	0.002
Brit. Aerospace	LG	30	-	0.002	0.001
SFENA, Франція	G-33	33	-	0.01	-
SFENA, Франція	Microgyro	12	-	1.0	0.07

1.4.1. Introduction to Fiber-optic gyros (FOG) in Aerospace Applications

A fiber-optic gyroscope (FOG) functions as an optoelectronic device for measuring absolute angular velocity relative to inertial space, operating on the principles of the Sagnac effect [8].

FOGs have gained significance in modern gyro technologies, supplanting traditional electromechanical gyroscopes. Despite laser gyroscopes being prevalent in aerospace applications, their reliability is compromised due to the use of gas lasers and high-voltage signals for drive control. GPS and MEMS gyroscopes serve as alternative navigation and inertial technologies but are often reserved for applications not demanding high accuracy due to limitations in precision, speed, and reliability. Moreover, atmospheric interference can impede GPS access.

FOGs offer advantages such as the absence of moving parts, immediate readiness without the need for a conventional "warm-up" period, and variable sensitivity depending on the length of the fiber sensor winding. However, the size and cost characteristics of FOGs often constrain their utilization in demanding applications, primarily due to the requirement for polarization-maintaining fibers and transceiver devices [9].

The operational principle of an FOG is grounded in the Sagnac effect. Optical radiation from a source, passing through an X-coupler, enters an integrated optical circuit where it divides into two beams propagating along the fiber-optic loop in opposing directions. In a stationary loop, no phase difference exists between the beams ($\Delta\varphi s = 0$). However, rotation of the loop relative to the inertial reference frame induces a phase difference $\Delta\varphi s$ proportional to the gyroscope's rotation rate. This variation in phase difference leads to a change in the detected radiation power by the photodetector.

With the progression of aircraft and rockets during the 20th century, gyroscopes evolved beyond mere toys. Aircraft, capable of free rotation and

movement in all three dimensions, necessitate navigation requirements absent in ground vehicles or ships. Hence, pilots must continually ascertain the aircraft's orientation along three axes for effective control.

Unmanned rockets and aircraft impose an additional requirement: autonomous orientation and positional awareness. This need is addressed by the Inertial Guidance System (IGS), utilizing gyroscopes to determine orientation and angular motion, thereby enabling continuous monitoring and calculation of the vehicle's displacement from its initial point. The fundamental configuration of a fiber-optic gyroscope is depicted in Fig. 1.4.1.

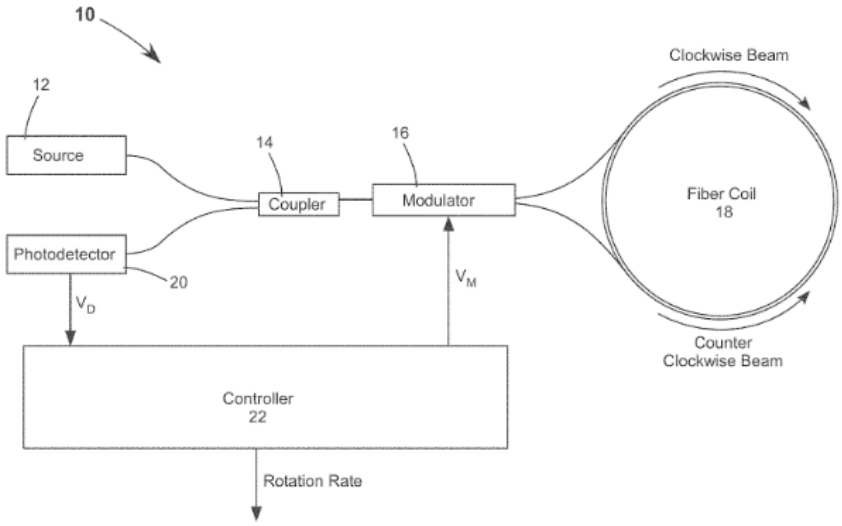

Fig. 1.4.1. The Basic Configuration of a fiber optic gyroscope (FOG)

The occurrence where light returning against the rotation direction arrives first happens because the sensor moves marginally closer to the moving beam during rotation. For example, in the described scenario, the left-traveling light beam returns before the right-traveling one. This time difference, termed phase shift, directly relates to the degree of rotation. This vital data is relayed downstream in various vehicles like aircraft, spacecraft, submarines, or missiles to uphold stability. These measurements occur at a rapid rate of 100 times per second, ensuring highly precise readings [10].

The initial gyroscopes were mechanical, comprising a rotating rotor propelled by a motor. Different sensors captured angular velocity and orientation data, transmitting it to the pilot or inertial guidance system (IGS). However, these mechanical gyroscopes were comparatively large and heavy, susceptible to vibrations, and necessitated frequent calibration.

Interferometric Fiber Optic Gyroscopes (IFOGs) emerged to address the constraints of mechanical gyroscopes. They employ an optical fiber coil, a coherent light source, and a photodetector to detect rotation, rather than a mechanical rotor. This yields smaller, lighter, and more accurate systems.

Within an IFOG, the light source splits into two beams before entering the fiber coil. These beams reunite at opposite ends of the fiber, with one rotating clockwise and the other counterclockwise. When the coil rotates around its axis, both beams encounter a phase shift relative to each other, known as the Sagnac effect.

Upon exiting the fiber, the two beams merge, generating interference fringes (bright and dark regions) in the combined beam due to any phase shift. A sensor detects this pattern to ascertain the angular velocity of rotation. Typically, three coils, each oriented at right angles to the other two, are employed to measure rotation along all three axes simultaneously [11].

FOG offers exceedingly precise rotational speed data, partly owing to its minimal lateral sensitivity to vibration, acceleration, and shock. Unlike traditional rotating mass gyroscopes or resonant/mechanical gyroscopes, FOG lacks moving parts and does not depend on inertial resistance to motion. This renders FOG a superb alternative to mechanical gyroscopes. Because of their reliability and extended lifespan, FOGs find applications in high-performance space endeavors [12] and military inertial navigation systems. A FOG typically exhibits higher resolution than a ring laser gyroscope.

FOGs can be employed in both open-loop and closed-loop configurations. Similar to all gyroscopic technologies, and contingent on the detailed FOG design, they may necessitate initial calibration to ascertain which indication corresponds to zero angular velocity.

Let's consider a photo (Fig. 1.4.2) of various fiber-optic gyroscopes.

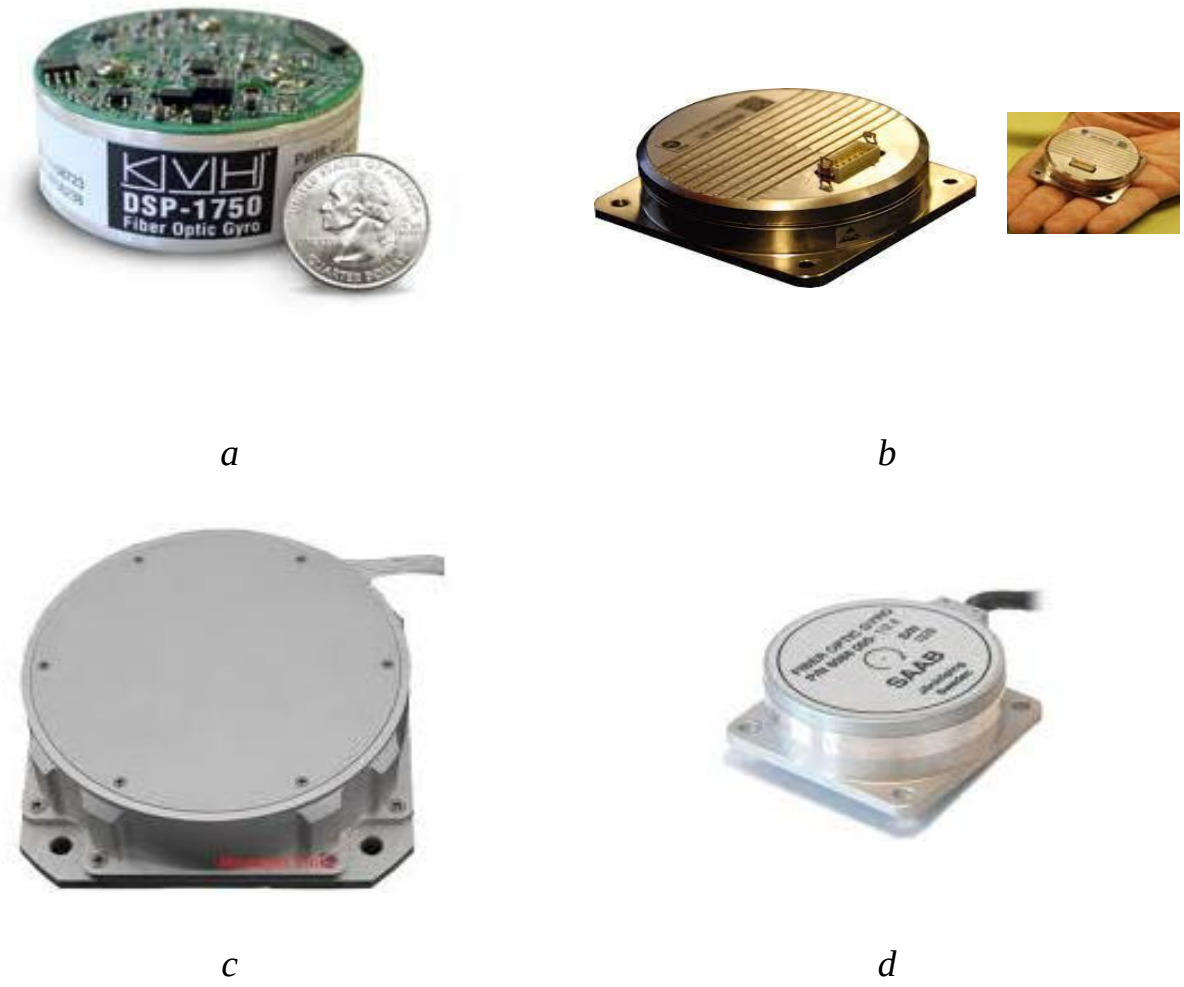

a *b*

c *d*

Fig. 1.4.2. Examples of the fiber-optic gyroscopes.

a – FOG of KVH Company, USA; *b* – Small-sized FOG of Patria Company, Netherlands; *c* – 15 cm diam. precision (0.003 deg/h) FOG of Newsigar Company, China; *d* – Small-sized FOG of Saab Company, Sweden

1.4.2. Inertial Measurement Unit (IMUs) based on FOG

Here are a few examples of inertial measurement devices based on Fiber-optic Gyroscopes:

Inertial Navigation System (INS): Inertial navigation systems that incorporate Fiber-optic Gyroscopes are commonly used in aircraft and other vehicles to precisely determine the vehicle's position and orientation [13].

Gyrocompasses: Fiber-optic Gyrocompasses are used in ships and other marine vessels to accurately determine their heading by measuring the rotation of the Earth [14].

Tactical-grade Gyroscopes: High-precision Fiber-optic Gyroscopes are used in a variety of military and aerospace applications, such as missile guidance systems and attitude control systems for spacecraft [15].

Example of the Inertial Measurement Unit (IMU) based on FOG is HG2802 Fiber Optic Gyro Inertial Measurement Unit (Fig. 1.4.3).

Fig. 1.4.3 HG2802

The HG2802 is a variant with an extended operating range within the HG2800 family of high-performance tactical-grade IMUs. It incorporates next-generation

Honeywell accelerometers with Micro-Electro-Mechanical Systems (MEMS) in addition to Fiber Optic Gyroscopes (FOG) with a closed-loop design, providing improved dynamic range and scale factor linearity. These IMUs are designed to meet the needs of a wide range of applications for pointing and control.

Due to their compact size, lightweight, wide bandwidth, low noise levels, and maintenance-free operation, the HG2800 IMUs are ideal for Electro-Optical (EO)/FLIR stabilization, camera/radar stabilization, pointing and positioning, mapping/inspection, autonomous underwater vehicle (AUV) and UAV navigation, odometer/DVL, as well as noiseless operation for acoustically sensitive systems. Table 3 shows the characteristics of this IMU [16].

Table 3

HG2802 IMU typical key characteristics

Diameter	3.5 in (8.89 cm)
Height	3.35 in (8.50 cm)
Weight	1.76 lbs (0.80 kg)
Power Consumption	7 W Nominal (10 W Max)
Operating Temperature Range	-40°C to +71°C
Data Rate	200 Hz (Guidance) and 1200 Hz (Control) — Other data rates available
Standard Interface Protocol	SDLC RS422
Gyro Operating Range	Standard ± 900°/sec
Accelerometer Operating Range	Standard ± 60g – Extended range ± 80g
Supply Voltages	Single +15VDC, or Dual +15VDC & +5VDC
Bandwidth @ 3dB	Standard: >100 Hz – Option: >300 Hz

The top FOG manufacturers are known for their high-pressure fog and misting systems used in a variety of applications. These systems are designed to provide adiabatic cooling, humidification, dust control and special effects, making the manufacturers world leaders in the production of high-quality high-pressure fog systems. Table 4 represent the FOG manufacturers and features.

Table 4

World leading FOG manufacturers and FOG main parameters.

Company, Country	Fiber length (m)	Dimension diam× height (mm)	Bias instability deg/h	Random walk $deg/h^{1/2}$	Scale factor temperature instability. % (1σ)	Measurement range deg/s
Litef (K-2030) Germany	-	80×33	0.1	0.02	0.03	1000
Litef (K-2010) Germany	100	37×25	36	1.0	1.0	1000
Stand.Electr. Lorenz AG Germany	100	80×26	10	0.16	0.5	400
Honeywell USA	140	70×30	0.1	0.003	-	-
Honeywell USA	685	126×28	0.03	0.006	0.2	50

1.5.1. Introduction to Vibratory Gyros with quarts resonators (HRG) in Aerospace Applications

The Hemispherical Resonator Gyroscope (HRG), also referred to as the Wineglass Gyroscope or Mushroom Gyroscope, stands out as a compact, low-noise, and high-performance sensor designed to measure angular velocity or rotation. Widely utilized in various applications ranging from spacecraft to guided missiles,

the HRG serves as a high-precision inertial navigation technology. Its primary advantage over alternative gyroscopic technologies lies in its remarkable reliability, durability, and accuracy [17].

The HRG (depicted in Fig. 1.5.2) is constructed using a thin semiconductor hemispherical shell affixed to a sturdy shaft. This shell undergoes resonance through the application of bending electrostatic forces generated by electrodes directly applied to individual fused-quartz structures surrounding the shell. The gyroscopic effect is achieved by leveraging the inertial properties of bending standing waves. Despite being a mechanical system, the HRG lacks moving parts, rendering it highly compact [18].

Fig. 1.5.1 Information about the gyroscope and its structure

One of the standout features of the HRG is its remarkable ability to uphold a stable resonance frequency across a broad temperature range. This achievement is

made possible through the utilization of a thermally compensated generator circuit, which adjusts the electrostatic driving force to sustain the necessary resonance frequency. The low coefficient of thermal expansion inherent in quartz material, coupled with the innate mechanical stability in hemispherical form, ensures exceptional frequency stability and, consequently, high accuracy in measuring angular velocities.

Due to its outstanding characteristics, the HRG has found extensive application in intricate systems demanding high precision and long-term reliability. Some of these applications include:

1. Spacecraft Navigation: HRGs are integrated into satellites and other spacecraft to facilitate position control and navigation, furnishing precise and stable orientation data for extended missions.

2. Missile Guidance: The exceptional precision and reliability of HRGs make them well-suited for incorporation into guided missile systems, enabling accurate target tracking and navigation.

3. Avionics: Both commercial and military aircraft leverage HRGs for navigation and flight control, providing vital data for autopilot systems and aiding in maintaining stable flight.

The hemispherical resonator gyroscope has emerged as a leading technology in the realm of inertial navigation due to its outstanding reliability, accuracy, and performance under challenging conditions. While the cost and power consumption may be higher compared to some competing technologies, the advantages of HRG render it a compelling choice for critical applications in spacecraft navigation, missile guidance, and avionics systems. It is anticipated that with further technological advancements, HRG will assume an increasingly significant role in the domain of inertial navigation and guidance [19].

The electronics responsible for sensing the standing waves also possess the capability to control them. As such, gyroscopes can function in either "full-angle

mode," determining the position of the standing waves, or in "force-balancing mode," maintaining the standing wave in a fixed orientation relative to the gyro.

Originally employed in space systems such as spacecraft attitude and orbit control systems, HRG has now found application in modern inertial navigation systems, position and heading reference systems, as well as HRG gyro compasses [20][21].

The first technological path in the development of gyroscopes led to the vibratory gyroscope with a hemispherical resonator made of quartz. Currently, these gyroscopes are manufactured by companies such as Northrop Grumman (USA) and Sagem (Safran) (France). Gyroscopes of this type are known for their outstanding capabilities in providing high accuracy, reliability, and durability. The complexity and high cost of manufacturing this technology urge researchers to seek an acceptable compromise between cost and accuracy. In the Fig. 1.5.2 we can see the types of resonators.

Fig. 1.5.2. Resonators made of fused quartz: a) a glass with 32 teeth; b) a mushroom-shaped resonator coated with a chromium film; c) a resonator assembled with a stem by deep optical contact

1.5.2. Inertial Measurement Unit (IMUs) based on HRG

Inertial Measurement Units (IMUs) based on HRG (Horizontal Ring Gyroscope) technology are used for measuring and tracking the orientation, position, and motion of objects in various applications.

HRG-based IMUs utilize the concept of gyroscopes to measure angular velocity and accelerometers to measure linear acceleration. The HRG technology specifically refers to the use of a horizontal ring-shaped gyroscope to detect rotational movement.

Inertial measuring module IVM-25L

The purpose of the IVM-25L is to be used as part of navigation systems as an autonomous measure of angular velocities and linear accelerations of highly dynamic moving objects. Structurally, the IVM-25L is based on three TVG-25 and a three-axis MEMS accelerometer (manufactured by Analog Devices), as shown in Fig. 1.5.3.

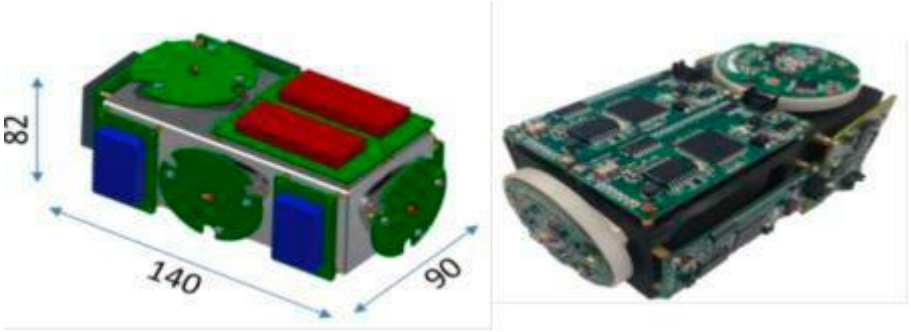

Fig. 1.5.3. Model and prototype of IVM-25L

Inertial measuring module IVM-25M

The purpose of the IVM-25M is to be used as part of navigation control systems as a measure of angular velocities and linear accelerations for objects with long periods of autonomous operation (Fig. 1.5.4). Structurally, the IVM-25M is based on three TVG-25 and three pendulum accelerometers (made in Ukraine/China).

Inertial measuring module IVM-43

IVM-43 is optimal for use in integrated navigation systems for solving navigation problems of moving objects with high accuracy (Fig. 1.5.5) [22].

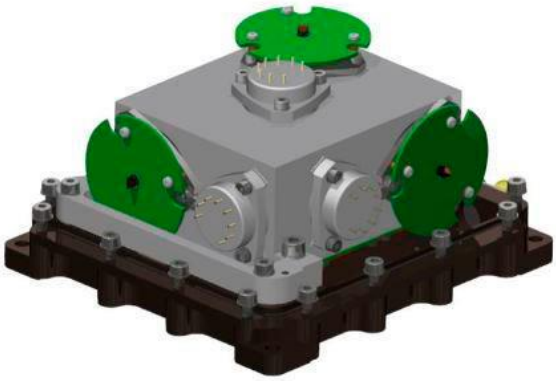

Fig. 1.5.4. Model IVM-25M

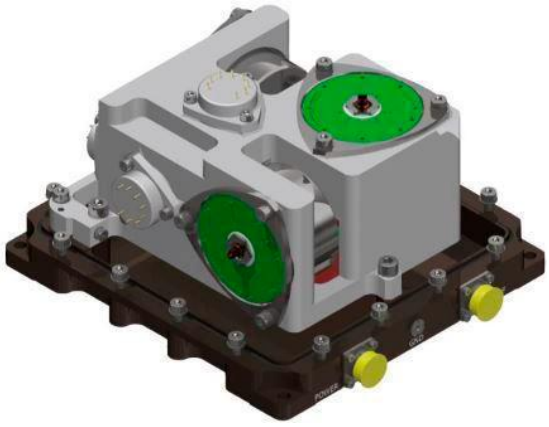

Fig. 1.5.5. Model IVM-43

HRG-based IMUs have several advantages over other types of gyroscopes. They offer high accuracy and precision, stability, and a longer lifespan than other technologies. In addition, they are resistant to shock, vibration, and temperature fluctuations, making them suitable for use in harsh environments such as aerospace, defense, and robotics.

Some popular manufacturers of HRG-based IMUs include:

1. Northrop Grumman - Their HRG-based IMUs are used in the aerospace and defense industries and are known for their high performance and reliability.
2. Honeywell - Honeywell offers HRG-based IMUs that are used in a wide range of applications.
3. KVH Industries - KVH is another well-known manufacturer of HRG-based IMUs used in areas such as autonomous vehicles, robotics, and maritime navigation.

1.5. Conclusion

As a result, today's high-quality gyroscopes play a crucial role in a variety of industries and applications that require precise measurement of orientation, position and motion. The three most common types of high-quality gyroscopes are ring laser gyroscopes (RLGs), fiber optic gyroscopes (FOGs) and quartz resonator gyroscopes (HRGs).

RLGs provide high accuracy and reliability, making them suitable for aviation, navigation and defense applications. They can provide reliable performance even in harsh environments.

FOGs are known for their compact size, reliability, shock and vibration resistance. They are widely used in industries such as autonomous vehicles, robotics, and aerospace.

HRGs use vibrating quartz resonators to measure rotation, providing excellent stability and long service life. They are often used in navigation systems for unmanned vehicles and aerospace applications.

Manufacturers of these high-quality gyroscopes include large companies with extensive experience, such as Honeywell, Northrop Grumman (formerly Litton) and KVH Industries, as well as smaller specialized companies.

The inertial measurement units (IMUs) based on these gyroscopes combine gyroscopic and accelerometric measurements to provide accurate and reliable orientation and motion data. These IMUs are used in a variety of industries, including aerospace, defense, robotics, and autonomous systems.

When selecting a high-quality gyroscope or IMU, factors such as accuracy, stability, environmental resistance, and specific application requirements should be considered.

Overall, the continued development of high-quality gyroscopic technology is helping to improve navigation, control and situational awareness in mission-critical applications, driving innovation and enabling further progress across a variety of industries.

SECTION 2

THE ALLAN VARIATION ANALYSIS METHOD

2.1. Introduction to Allan Variance

Measuring the accuracy and stability of sensors and measuring systems is a fundamental task of modern science and technology. In this regard, there is a need for sophisticated methods for analyzing and modelling random errors.

Allan's method of variational analysis stands out as a widely used and effective approach for assessing the variational stability of measurement systems. It facilitates the study of the characteristics of random errors in measuring instruments, allows you to determine their main parameters and build models that illustrate their impact on measurement accuracy.

This chapter delves into the random error models defined by the Allan bell curve. Starting with an overview of the primary models of noise and error, the discussion moves on to their mathematical analysis and impact on measurement accuracy. The use of the Allan analysis of variance method not only allows for the identification of random errors, but also helps to develop effective strategies to reduce and correct them.

The essence of this chapter is a comprehensive understanding of the variational stability of measuring systems using the Allan's analysis of variation method, as well as the study of new approaches to modelling and controlling random errors.

2.2. Typical Allan Deviation Plot

The Allan deviation plotted against cluster time (T) is typically visualized using a log-log graph. The Allan variance curve typically exhibits a U-shaped pattern. Fig. 2.2.1 depicts a typical Allan deviation curve observed during the analysis of a stationary inertial sensor's output.

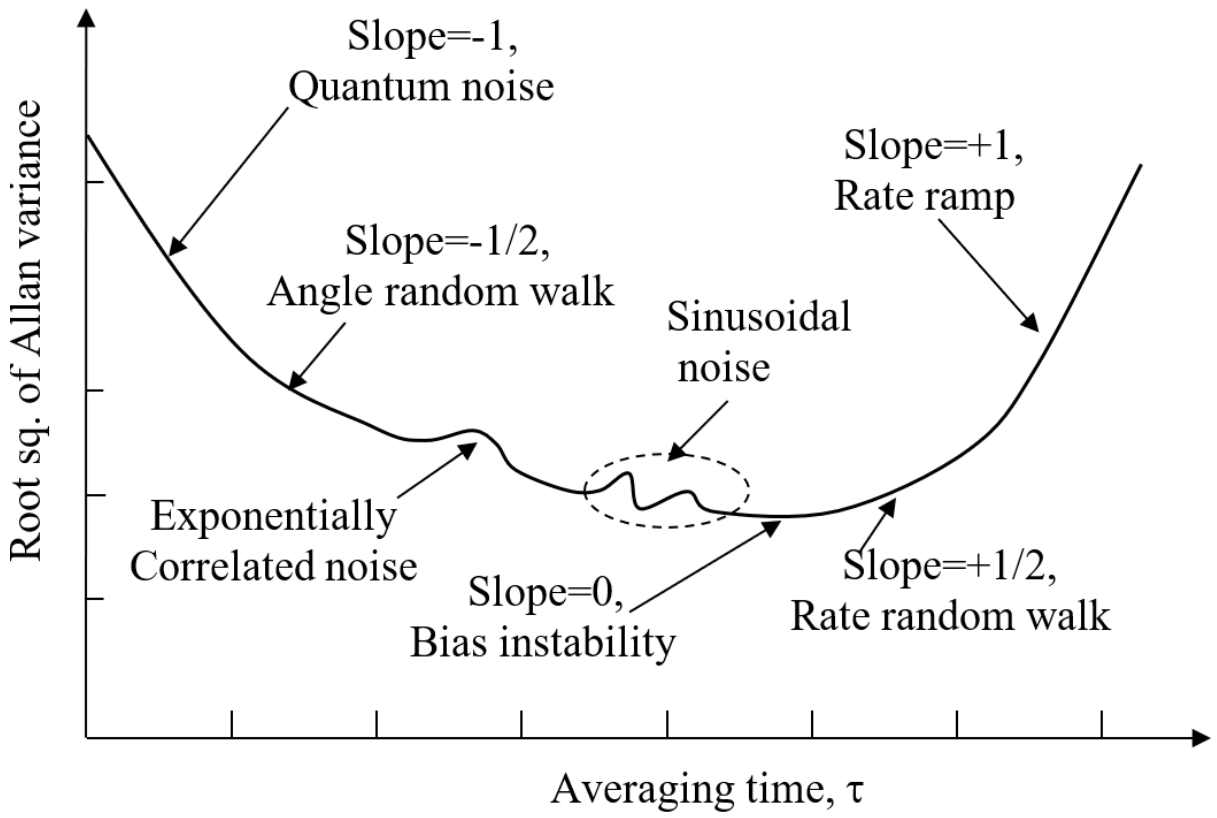

Fig. 2.2.1. Typical square root of the Allan variance versus averaging time

The x-axis (T) corresponds to time units such as microseconds, seconds, minutes, or hours, while the y-axis denotes angular velocity (e.g., rad/s or °/h) for gyroscopes or acceleration (in g or m/s2) for accelerometers. It is evident that the slope of the curve varies depending on the cluster time (T).

In essence, the Allan variance provides a means to discern and measure different noise components present in the data [23].

2.3. Allan Variance: description of random error models

The Allan Variance (AVAR), also referred to as the two-sample variance, acts as a metric for frequency stability in clock generators, oscillators, and amplifiers. It derives its name from David W. Allan. Mathematically, it is represented as follows:

$$\sigma_y^2(\tau).$$

The Allan Deviation (ADEV) is defined as the square root of the Allan Variance and is alternatively known as sigma-tau. Mathematically, it is expressed as follows:

$$\sigma_y(\tau).$$

The M-sample variance is a metric for frequency stability that considers M samples, the time interval T between measurements, and the observation time. It is mathematically expressed as follows:

$$\sigma_y^2(M, T, \tau).$$

The Allan Variance focuses on assessing stability related to noise processes rather than systematic errors or imperfections such as frequency drift or temperature effects. Both the Allan Variance and Allan Deviation are indicators of frequency stability [24].

In simpler terms, the Allan Variance is a technique used to represent the root mean square errors caused by random drift in relation to averaging time. It is straightforward to calculate and relatively easy to interpret and comprehend. The Allan Variance method aids in identifying the characteristics of underlying random processes that contribute to noise in data. In this context, the method is applied to

discern the characteristics of different noise types present in various inertial sensor data.

The Allan variance is estimated as follows:

$$\sigma^2(T) = \frac{1}{2T^2(N-2n)} \sum_{k=1}^{N_{-2n}} (\theta_{k+2n} - 2\theta_{k+n} + \theta_k)^2 \,. \#(2.1)$$

There is a unique relationship that exists between $\sigma^2(T)$ and the PSD of the intrinsic random processes. This relationship is

$$\sigma^2(T) = 4 \int_0^\infty df \cdot S_\Omega(f) \left(\frac{\sin^4(\pi f T)}{(\pi f T)^2} \right), \#(2.2)$$

where $S_\Omega(f)$ is the PSD of the random process $\Omega(T)$.

In deriving equation (2.2), it is assumed that the random process Ω(T) exhibits time-stationarity. This assumption ensures that the autocorrelation function of Ω(T) remains constant over time, with an even autocorrelation function being a crucial requirement for equation (2.2) derivation.

Equation (2.2) establishes a connection between the Allan variance and the total power output of the random process when subjected to a specific filtering operation represented by the transfer function $\sin^4(x)/(x)^2$. This transfer function mirrors the methodology employed in data clustering and processing.

Equation (2.2) serves as the cornerstone of the Allan variance method, facilitating the computation of Allan variance from the rate-noise Power Spectral Density (PSD). By substituting the PSD of any physically meaningful random process into the integral, one can derive an expression for Allan variance $\sigma^2(T)$ as a function of cluster length.

On the contrary, as $\sigma^2(T)$ is a measurable parameter, plotting σ(T) against T on a log-log scale offers insights into the nature of random processes within sensor data.

Although the Allan variance can be derived uniquely from the Power Spectral Density (PSD) of a stochastic process, there is no general inversion formula due to the absence of a one-to-one relationship between them. Detailed derivations regarding these concepts can be found in specified sources [25].

While Allan Variance statistics are valuable for detecting broad spectral trends, they do not always define a singular noise spectrum, given the lack of a one-to-one mapping from spectrum to Allan Variance. This fundamental limitation restricts the depth of knowledge that can be gleaned about the noise process solely from studying its Allan Variance.

Below is the mathematical definition of Allan Variance and the relationship between Allan Variance and Power Spectral Density (PSD). Using this relationship, the behavior of the characteristic curve for a range of known noise members can be determined.

The primary categories of random errors commonly analyzed within the framework of the Allan variance curve include:

1. Quantization white noise: This represents the inherent noise introduced during signal measurement and processing, particularly in digital systems.
2. Angular random walk: This type of error characterizes the non-linear drift of a measuring instrument over time.
3. Correlated noise: Refers to noise where the current value of a variable depends on its past values, indicating a certain level of correlation over time.
4. Periodic noise: This type of noise exhibits periodic fluctuations in its magnitude, repeating at regular intervals.
5. Bias instability: This error signifies the variation in the measuring instrument's output over time, often attributed to factors like drift or instability.
6. Random walk rate: This describes the rate at which a variable's value changes over time, indicating the speed of random fluctuations.

7. Velocity ramp: Represents errors caused by changes in velocity or speed over time, contributing to variations in measurement outputs.

The following section will present the comprehensive solution for various specific noise types, which are known to exist in inertial sensors or are believed to impact the data.

Quantization noise pertains to the discrepancy introduced during the conversion of an analog signal into digital format. This error originates from the minor disparities between the actual amplitudes of sampled points and the resolution of the analog-to-digital converter. For instance, within the context of a gyroscope output, the angle power spectral density (PSD) stemming from quantization noise is delineated as follows:

$$S_\theta(f) = T_s Q_z^2 \left(\frac{\sin^2(\pi f T)}{(\pi f T)^2} \right) \approx T_s Q_z^2, f < \frac{1}{2T_s}, \#(2.3)$$

where Q_z quantization-noise coefficient;

T_s sample interval.

The theoretical limit for Q_z is equal to $S/12^{1/2}$, where S denotes the gyro scaling coefficient used in tests with consistent and uniform sampling intervals. The gyro rate power spectral density (PSD) is linked to the angle PSD through the following
correlation:

$$S_\Omega(2\pi f) = (2\pi f)^2 S_\theta(2\pi f), \#(2.4)$$

and is

$$S_\Omega(f) = \frac{4Q_z^2}{T_s} \sin^2(\pi f T s) \approx (2\pi f)^2 T_s Q_z^2, \qquad f < \frac{1}{2T_s}. \#(2.5)$$

Substituting (2.5) into (2.2) and performing the integration yield

$$\sigma^2(T) = \frac{3Q_z^2}{T^2}. \# (2.6)$$

The behavior of quantization noise is depicted by a log-log plot of *σ(T)* against *T*, displaying a slope of -1 as illustrated in Fig. 2.3.1. In this figure, the time axis is represented in units relative to the sample time t0. The magnitude of this noise can be determined by observing the slope of the line at $T = 3^{1/2}$.

Additionally, it's important to acknowledge the presence of other noise types with varying spectral characteristics, such as flicker angle noise and white angle noise. These noise types exhibit the same Allan variance dependence on *T* as quantization noise.

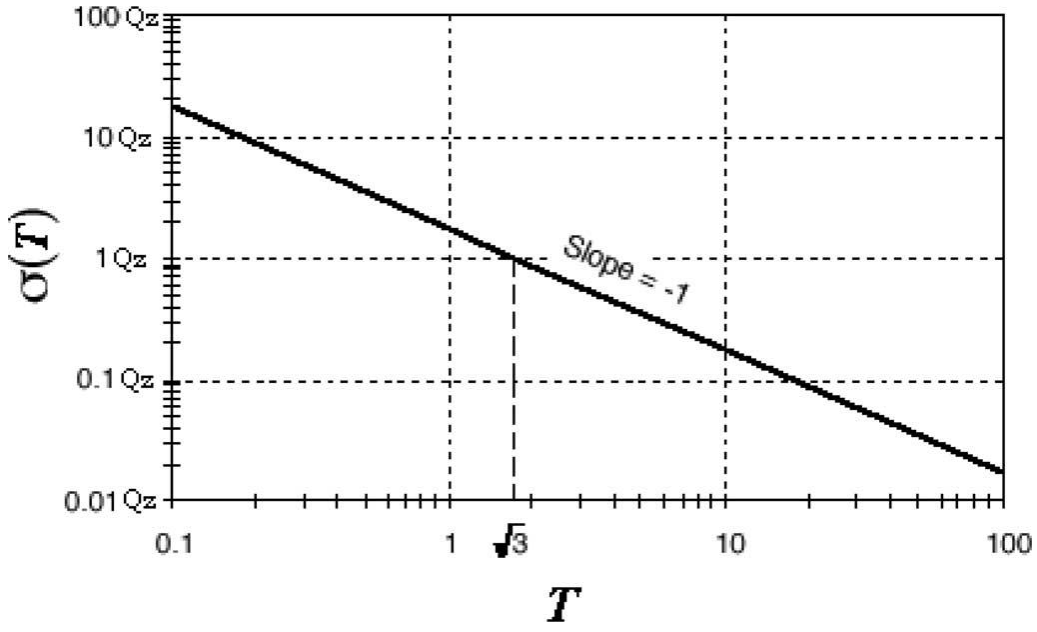

Fig. 2.3.1. *σ*(*T*) plot for quantization noise

Angular (Velocity) Random Walk: Noise components characterized by high frequencies and correlation times significantly shorter than the sample time can impact the gyro's angle (or accelerometer's velocity) random walk. However, effective design strategies can often mitigate most of these sources. These noise components typically manifest as a white-noise spectrum in the gyro's (or

accelerometer's) rate output. The corresponding rate noise Power Spectral Density (PSD) is expressed as:

$$S_\Omega(f) = Q^2, \#(2.7)$$

where Q is the angle (velocity) random-walk coefficient.

Substituting (2.7) into (2.2) and performing the integration yield

$$\sigma^2(T) = \frac{Q_z^2}{T}. \#(2.8)$$

As depicted in Fig. 2.3.2, equation (2.8) reveals that a log-log plot of $\sigma(T)$ against T displays a slope of -1/2. Moreover, the precise value of Q can be directly ascertained by analyzing the slope line at $T = 1$.

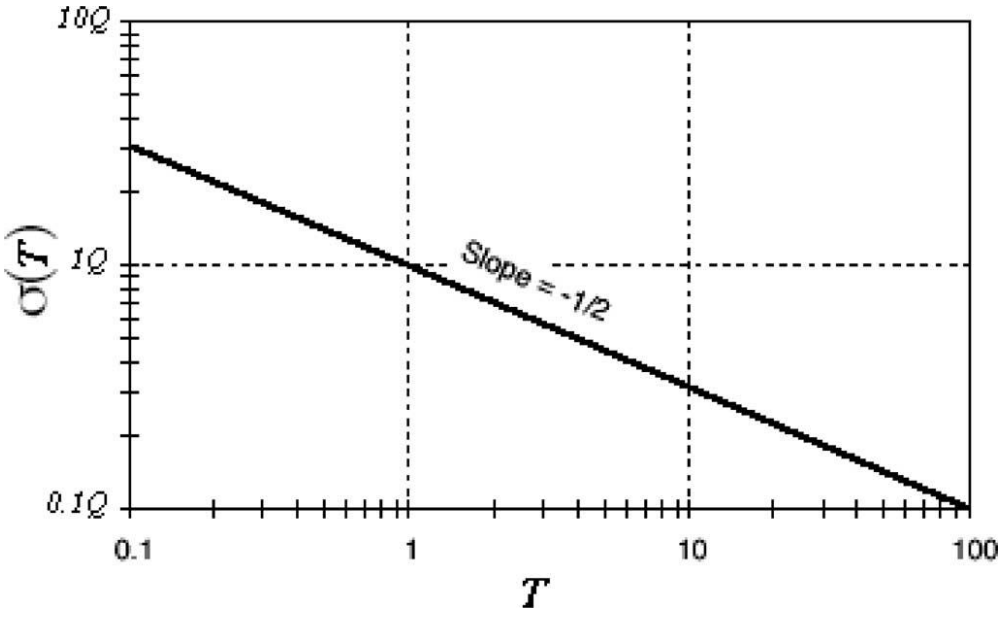

Fig. 2.3.2. $\sigma(T)$ plot for angle (velocity) random walk

Bias Instability: This form of noise arises from random fluctuations in electronic components or other elements, leading to variations in the bias within the data, primarily characterized by low-frequency characteristics. The Power Spectral Density (PSD) associated with this noise is delineated by the following equation:

$$S_\Omega f = \begin{cases} \left(\frac{B^2}{2\pi}\right)\frac{1}{f}, & f \le f_0 \\ 0, & f > f_0 \end{cases}, \#(2.9)$$

where B bias instability coefficient;

f_0 cutoff frequency.

Substituting (2.9) into (2.2) and performing the integration yield

$$\sigma^2(T) = \frac{2B^2}{\pi} \times$$

$$\left[ln\,2 - \frac{sin^3 x}{2x^2}\,(sin\,x + 4x\,cos\,x) + C_i(2x) - C_i(4x)\right], \#(2.10)$$

where $x = \pi f_0 T$;

C_i is cosine-integral function.

Fig. 2.3.3 displays a log-log plot of equation (2.10), illustrating that the Allan variance linked to bias instability reaches a plateau for significantly extended durations compared to the inverse cutoff frequency. Consequently, examining the flat segment of the plot enables the estimation of the bias instability limit.

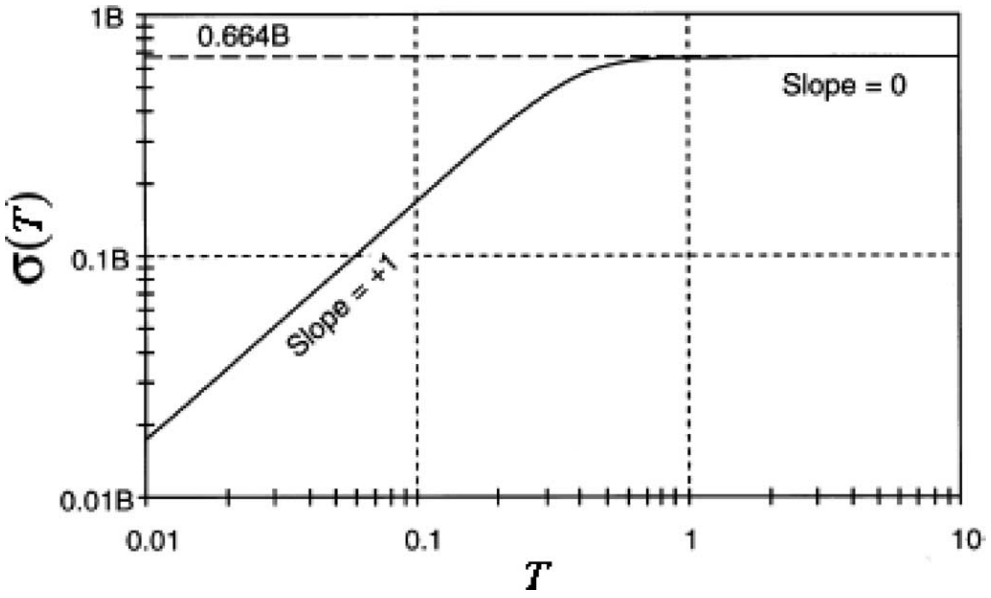

Fig. 2.3.3. $\sigma(T)$ plot for bias instability (for $f0 = 1$) [4] (the value 0.664 in the figure is the result of $\sqrt{2\ ln2/\pi}$)

Rate Random Walk: This phenomenon characterizes a random process with an uncertain origin, possibly resembling an extreme instance of exponentially correlated noise with an exceptionally prolonged correlation time. The Power Spectral Density (PSD) linked to this noise is expressed by the following equation:

$$S_\Omega(f) = \left(\frac{K}{2\pi}\right)^2 \frac{1}{f^2}, \#(2.11)$$

where K is the rate random-walk coefficient.

Substituting (2.11) into (2.2) and performing the integration yield

$$\sigma^2(T) = \frac{K^2 T}{3}. \#(2.12)$$

The rate random walk is visualized with a slope of +1/2 on a log-log plot of $\sigma(T)$ against T, as shown in Fig. 2.3.4. The magnitude of this noise, indicated as K, can be established by examining the slope line at $T = 3$.

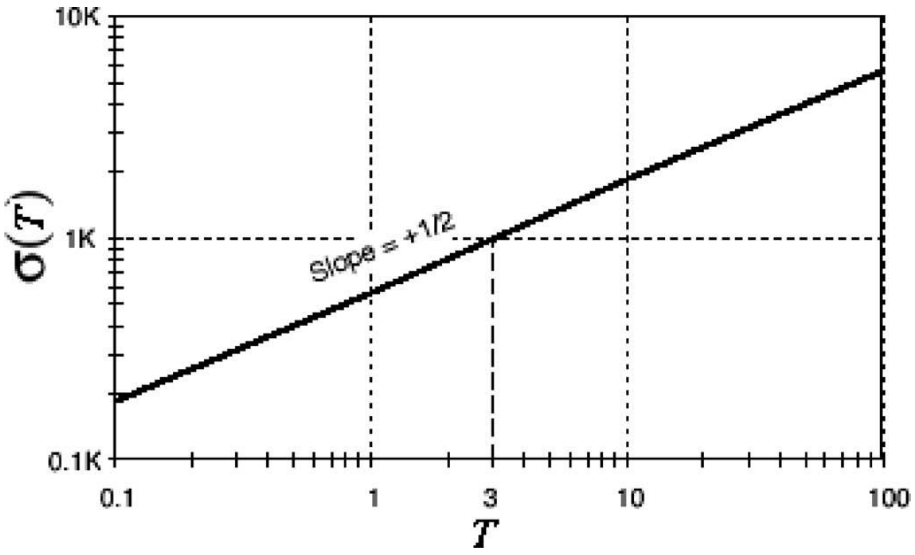

Fig. 2.3.4. $\sigma(T)$ plot for rate random walk

Drift Rate Ramp: In contrast to the random nature of previously discussed error terms, it is essential to consider how σ(T) responds to systematic or deterministic errors. One such error is the drift rate ramp, defined as:

$$\Omega = Rt, \#(2.13)$$

where *R* is the drift-rate-ramp coefficient.

By forming and operating on the clusters of data containing an input given by (2.13), we obtain

$$\sigma^2(T) = \frac{R^2T^2}{2}. \#(2.14)$$

This indicates that the drift-rate-ramp noise displays a slope of +1 in the log-log plot of *σ(T)* against *T*, as depicted in Fig. 2.3.5. The magnitude of the drift rate ramp, denoted as *R*, can be determined from the slope line at $T = 2^{1/2}$.

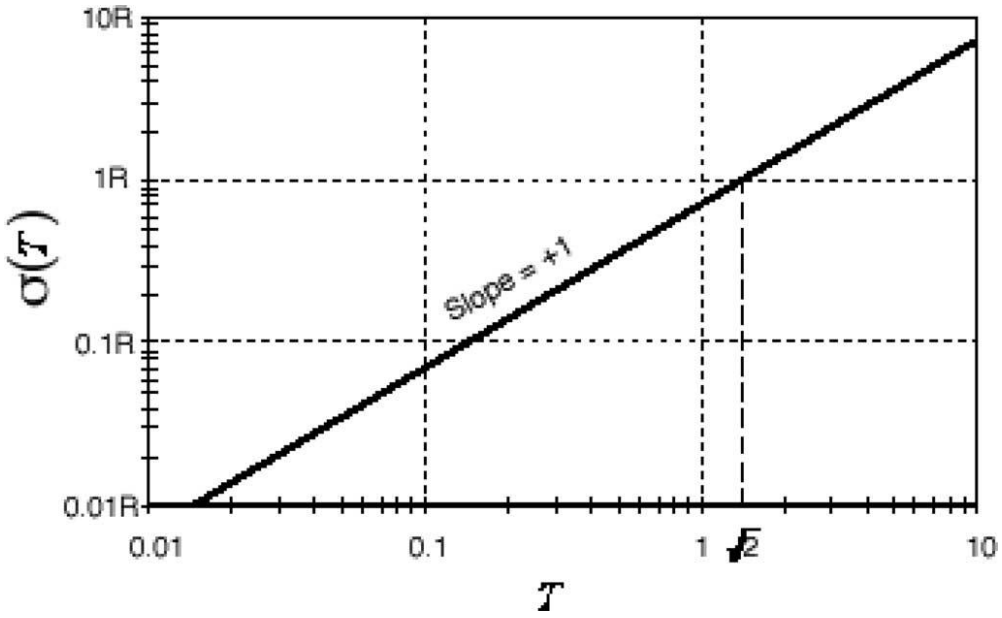

Fig. 2.3.5. *σ*(*T*) plot for drift rate ramp

The rate PSD associated with this noise is:

$$S_\Omega(f) = \frac{R^2}{(2\pi f)^3}. \#(2.15)$$

It should be noted that there might be a flicker acceleration noise with $1/f^3$ PSD that leads to the same Allan-variance *T* dependence [26].

A graph of a function $\sigma^2(T)$ (Allan variance) built by measurement data in log-log scale indicates a type of random component, which is in the gyro output signal. It is usually built a graph of a square root of the Allan variance $\sigma_\Omega(T)$ versus a length of time interval *T* (i.e. averaging time) on a log-log scale.

Different noise components appear on the Allan variance graph at different intervals of the averaging time variable *T*. This allows one to detect on the Allan curve various random components which are present in the measurement data. Assuming that the above noise components are independent of each other, the total Allan variance can be written as the sum of the variances of its components as follows:

$$\sigma_\Omega^2(T) = \frac{3Q^2}{n^2T^2} + \frac{N^2}{nT} + \frac{2ln2}{\pi}B^2 + M^2\sqrt{\frac{nT}{3}} + K^2\frac{nT}{3} + R^2\frac{n^2T^2}{2} + \\ + \Omega_0^2\left(\frac{sin^2(2\pi f_0 T)}{\pi f_0 T}\right)^2 . \#(2.16)$$

As can be seen from (Fig. 2.2.1), the contribution of each subcomponent to total noise is quantitatively determined by corresponding coefficients *Q*, *N*, *B*, *K*, and *R*. These coefficients are computed by the square root of the Allan variance graphed in log-log scale versus averaging time *T* such as described below.

Q is a random drift due to quantum noise measured in degrees (it is present only for digital gyroscopes);

N is a random drift due to angle random walk measured in deg/h$^{1/2}$ (or in deg/s$^{1/2}$ for low-cost gyros);

B is a random drift due to bias instability measured in deg/h (or in deg/s);

K is a random drift due to rate random walk measured in deg/h$^{3/2}$ (or in deg/s$^{3/2}$);

R is a random drift due to rate ramp measured in deg/h^2 (or in deg/s^2);

The *Q* value is determined as an ordinate of an intersection point of a tangential line with slope -1 (tanα=-1) to $\sigma_{\Omega}(T)$ curve and a vertical line originating from the point $T=3^{1/2}h$ (hour). It is measured in degrees. If Q value for $T=3^{1/2}$ h is located out of graph frame, then $T=3^{1/2}$ *s* can be taken and, in this case, *Q* is measured in arcsec.

The *N* value is determined as an ordinate of an intersection point of a tangential line with a slope -0.5 (tanα=-0.5) to $\sigma_{\Omega}(T)$ curve and a vertical line originating from the point *T*=1 *h*. It is measured in deg/h$^{1/2}$.

The *B* value is determined as an ordinate of a minimum of a $\sigma_{\Omega}(T)$ curve (it's flat part) divided by a constant 2ln2/π≈0.664. It is measured in deg/h.

The *M* value is determined from the following equations:

$$\sigma_{\Omega}(T_M) = 0.437\mathrm{M}\sqrt{T_c}\ ;\ T_c = 1.89/T_M, \#(2.17)$$

where T_c is a correlation time of exponentially correlated noise, and T_M is an averaging time at which $\sigma_{\Omega}(T_M)$ is a local maximum of the convexity indicated in Fig. 9.2. The correlation function $C_M(t)$ of the exponentially correlated noise is:

$$C_M(t) = Me^{\frac{t}{T_c}}. \#(2.18)$$

M dimension is deg/c$^{3/2}$, or deg/h$^{3/2}$, 1 deg/c$^{3/2}$=2.16*10^5 deg/h$^{3/2}$.

The *K* value is determined as an ordinate of an intersection point of a tangential line with a slope of 0.5 (tanα=0.5) to $\sigma_{\Omega}(T)$ curve and a vertical line originating from the point *T*=3 *h*. Its dimension is deg/h$^{3/2}$. If *K* value for *T*=3 h is located out of graph, then *T*=3 *s* can be taken, and in this case, *K* dimension is deg/h/s$^{1/2}$, deg/h/s$^{1/2}$=60 deg/h$^{3/2}$.

The *R* value is determined as an ordinate of an intersection point of a tangential line with a slope +1 (tanα=1) to $\sigma_{\Omega}(T)$ curve and a vertical line originating from the point $T=2^{1/2}\,h$.

The Ω_0 value is determined from the following equations:

$$\sigma_{\Omega}(T_s) = 0.725\Omega_0;\ f_0 = 0.371/T_s, \#(2.19)$$

where Ω_0 and f_0 are the amplitude and frequency of a sinusoidal noise;
T_s is an averaging time at which $\sigma_{\Omega}(T_s)$ is a maximum (the first one) of the consecutive picks fall off rapidly in increasing of the averaging time *T*.

2.4. Interpretation of the Allan Variance Curve

The interpretation of the Allan Variance curve involves understanding its three distinct parts (Fig. 2.4.1).

The first part of the curve exhibits a negative gradient slope from the initial point, denoted as σ, to points close to the minimum. Each point, denoted as $\sigma^2(1)$, represents the deviation or variance of a set of averaged values derived from the dataset.

For instance, the second point on the Allan Variance curve corresponds to the set of running averaged values $(x_m + x_{m+1})/2$ for all i in $\mathbb{N}$.

Averaging over 2 samples results in the suppression of the highest frequency noise components. Consequently, the deviation represented by the second point on the curve is generally lower than that of the first point, and similarly, the third point exhibits a lower deviation than the second, and so forth.

The second part of the Allan Variance curve encompasses the region around and including the minimum point. Normally, one would anticipate that averaging over larger numbers of samples would progressively reduce the variance and deviation of the set of averaged samples, approaching zero in an exponential manner.

However, in systems with non-convergent noise, this reduction doesn't occur as expected, and there are several reasons for this divergence.

The third part of the Allan Variance curve consists of the region where the gradient slope becomes positive, rising from the minimum point. This rise is primarily due to the increasing significance of 1/f noise and other low-frequency noise sources like random walk at low frequencies and long sampling times. When sample averages are taken over very low frequencies but less than a full cycle, they generally exhibit a distribution of values ranging from the maximum amplitude of the low-frequency components to the minimum. This distribution of values across a band of low frequencies contributes to a measurable noise distribution, leading to the observed rise in the Allan Variance curve.

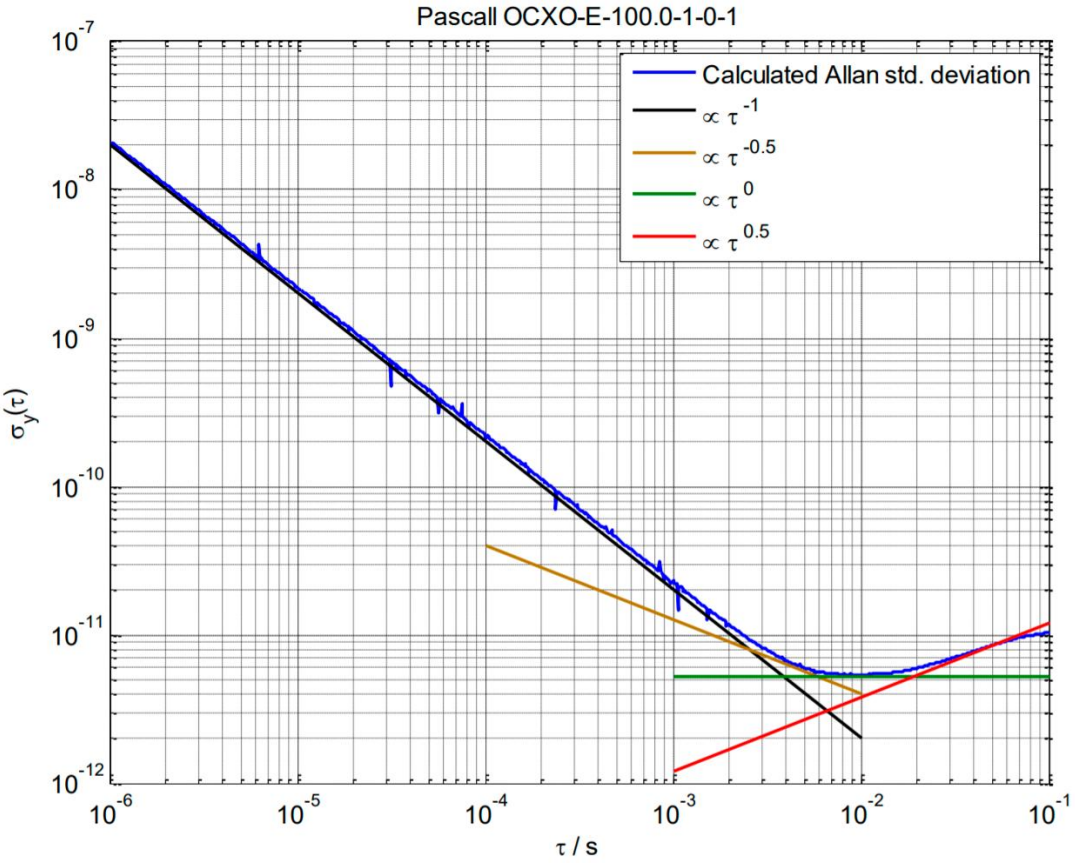

Fig. 2.4.1. Graph of Allan Deviation for an oven-controlled oscillator with marked up noise processes

The Allan Variance and its interpretation are influenced by several key factors related to the measurement process:

1. **Total Measurement Time (T_{meas})**: This refers to the overall duration of measurement during which a certain number of samples, denoted as n, are collected or computed.

2. **Sampling Time (T_s)**: This is a constant value specific to each Allan Deviation calculation. It determines the time interval between consecutive samples.

3. **Maximum Number of Time-Averaged Samples (n_s)**: This is the maximum number of samples that can be averaged during the total measurement time T_{meas} for a given sampling time T_s, calculated as $n_s = T_{meas} / T_s$.

4. **Effect of Sampling Time on Noise**: As the sampling time Ts increases, the high-frequency cutoff of the algorithmic low-pass filter decreases. This means that higher frequency noise components are averaged out more effectively with longer sampling times, assuming the noise is convergent.

5. **Contribution of Noise to Allan Deviation**: For the shortest sampling time T_1, the noise contributing to the Allan deviation includes all frequency components limited by the sample averaging time. As the sampling time increases (s > 1), higher frequencies are averaged away, and the variance due to noise primarily reflects the sum of lower frequency noise components.

6. **Two-Sample Deviation**: This measure captures the deviation between successive averaged samples. It effectively captures noise frequencies equal to or greater than $\frac{1}{\text{two sample periods} + \text{any dead time}}$.

7. **Influence of Sampling Frequency on Deviation**: The two-sample deviation increases as the sampling period increases or as the sampling frequency decreases, provided the sampling period is less than the period of the noise frequencies of interest.

8. **Low-Frequency Noise and Deviation**: The amplitude (or power) of 1/f noise rises inversely with frequency. Therefore, the two-sample deviation increases as the sampling period increases (or sampling frequency decreases), especially for low-frequency noise sources.
9. **Low-Frequency Cut-Off**: There is a low-frequency cut-off determined by T_{meas}. Frequencies significantly lower than $\frac{1}{T_{meas} \times 4}$ contribute less to signal deviation due to their slow-changing nature.
10. **Significance of Low-Frequency Noise**: In systems where low-frequency responses are critical, such as those affected by slow-changing environmental factors (e.g., temperature variations over long periods), low-frequency noise sources like 1/f noise become significant and contribute to the variance as T_{meas} increases [27].

2.5. The practical example

As a practical example, let's consider the square root of Allan variance of the TVG-25 of Ukrainian producer presented in Fig. 2.5.1.

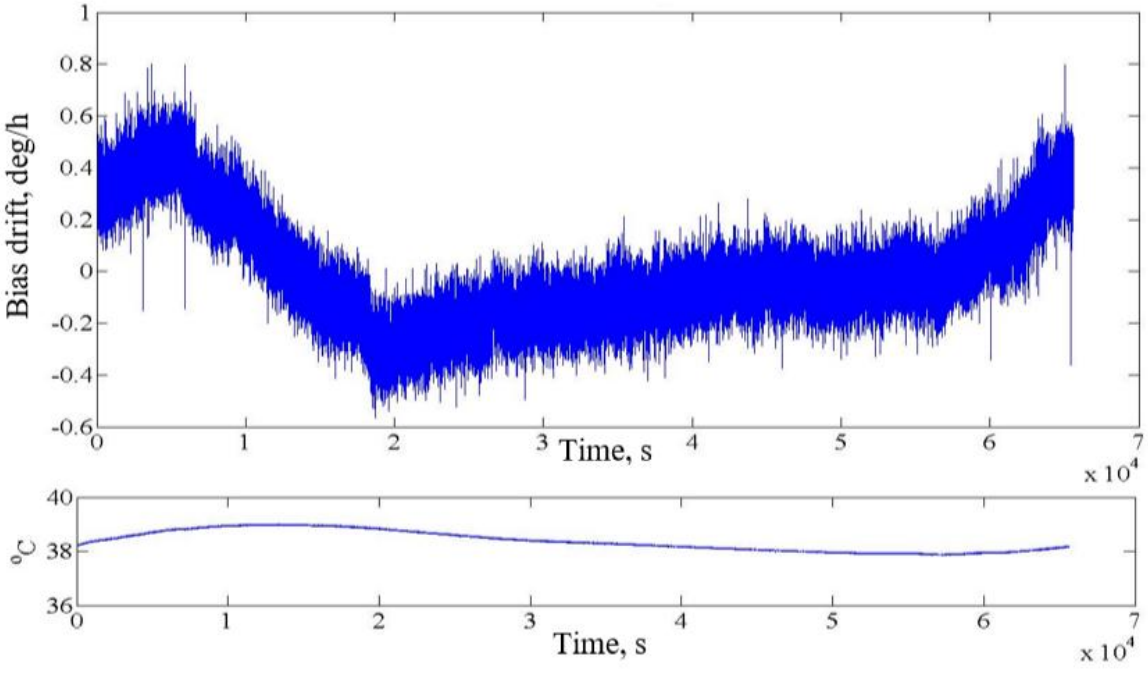

Fig. 2.5.1. TVG-25 Bias drift and temperature versus time

Fig. 2.5.2 shows root square (standard deviation) of Allan variance TVG-25 gyro output signal in static shown in Fig. 2.5.1.

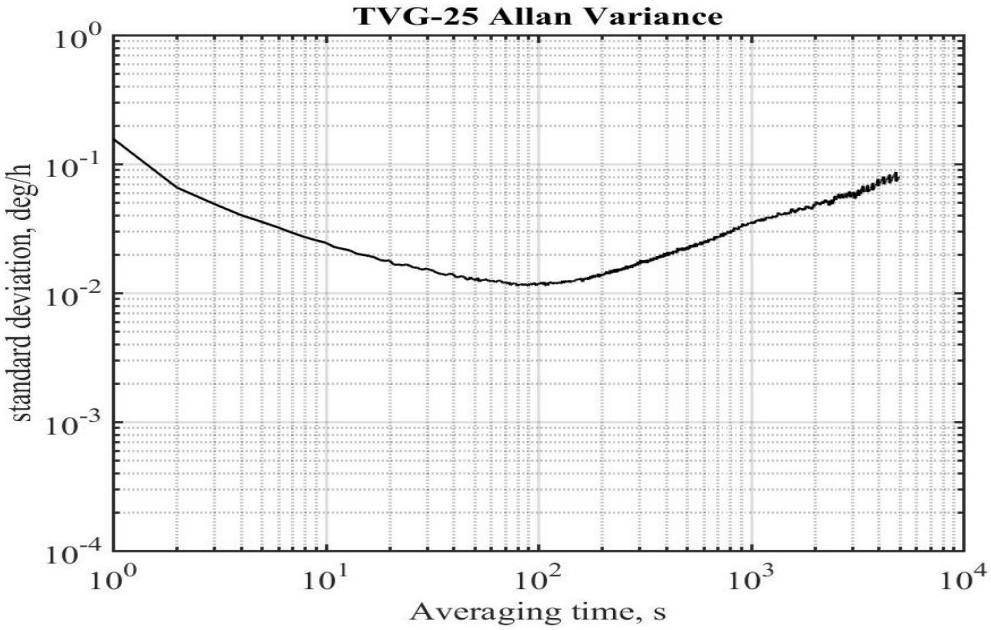

Fig. 2.5.2. TVG-25 root square of Allan variance, $\sigma_{\Omega}(T)$

Example of quantum noise coefficient *Q* determination in correspondence to abovementioned description is presented in Fig. 2.5.3.

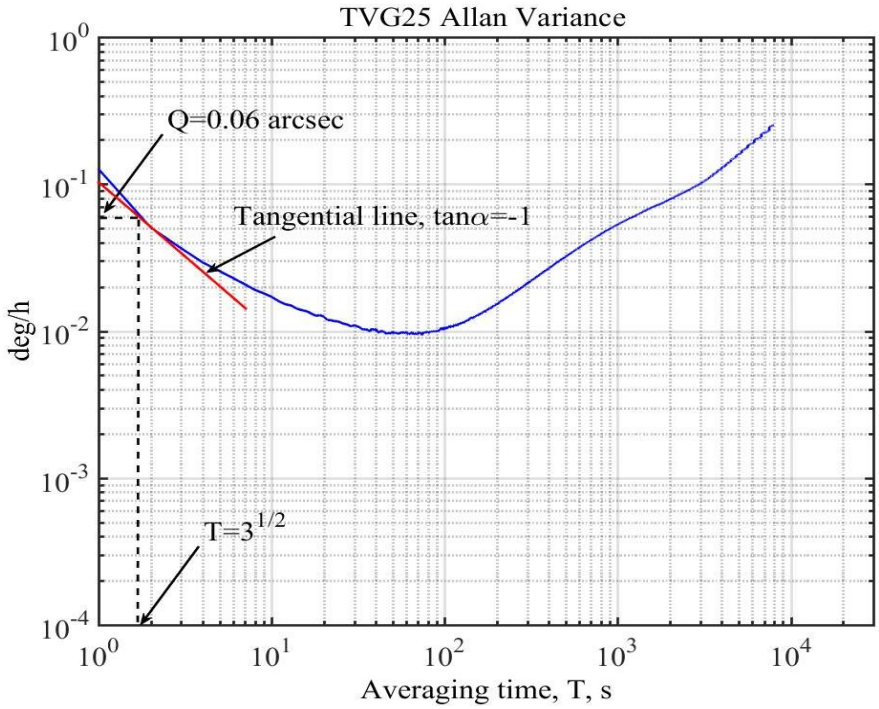

Fig. 2.5.3. Determination of quantum noise for TVG-25

Example of random walk coefficient N determination in correspondence to abovementioned description is presented in Fig. 2.5.4.

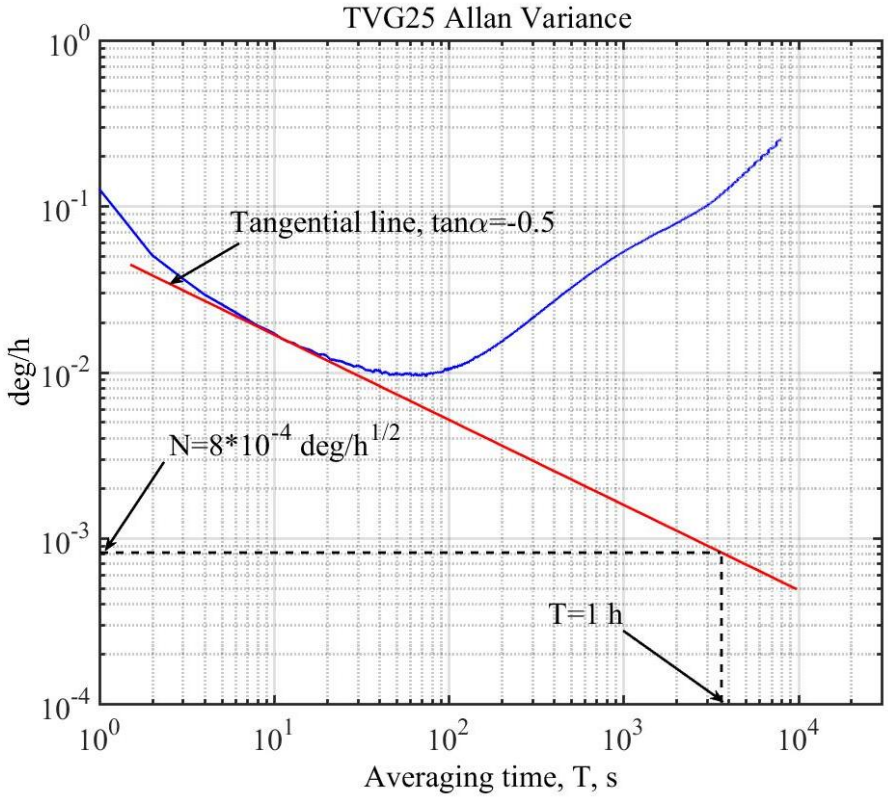

Fig. 2.5.4. Determination of random walk for TVG-25

Example of a bias instability coefficient *B* determination in correspondence to abovementioned description is presented in Fig. 2.5.5.

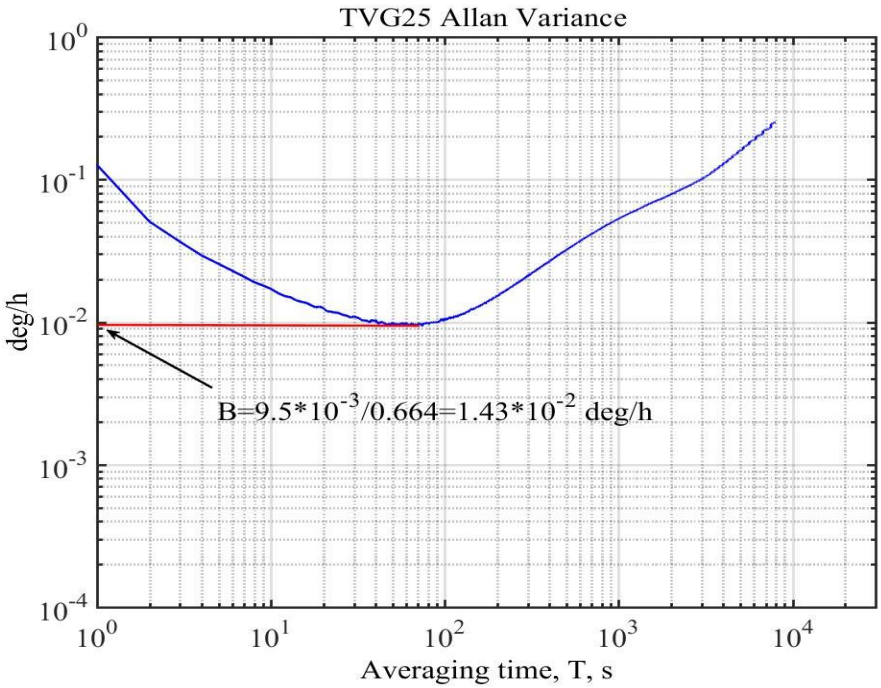

Fig. 2.5.5. Determination of bias instability for TVG-25

Example of a rate random walk coefficient *K* determination in correspondence to abovementioned description is presented in Fig. 2.5.6.

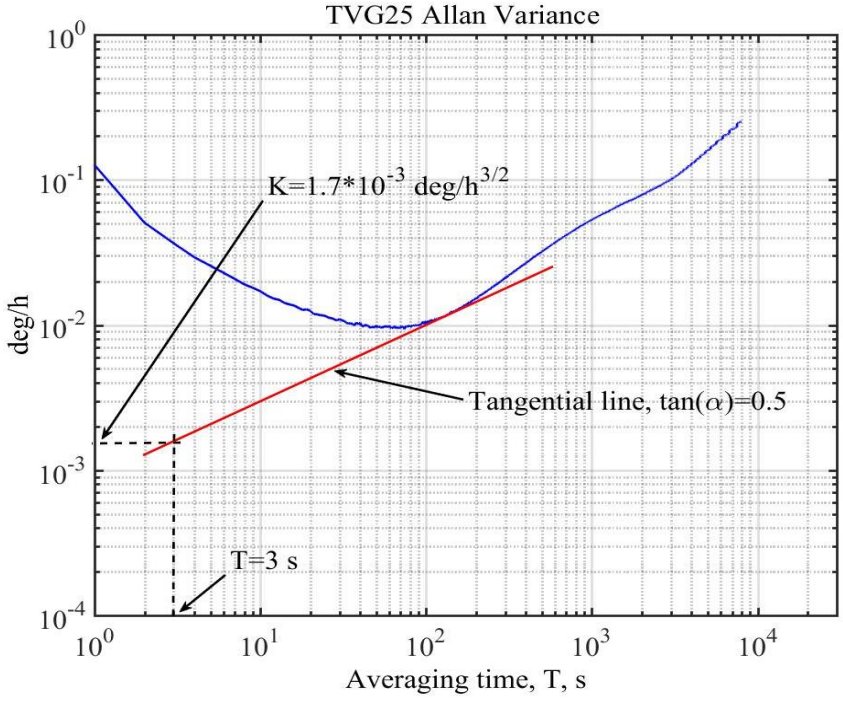

Fig. 2.5.6. Determination of rate random walk for TVG-25

Example of a rate ramp (trend in measurement data) coefficient *R* determination in correspondence to abovementioned description is presented in Fig. 2.5.7.

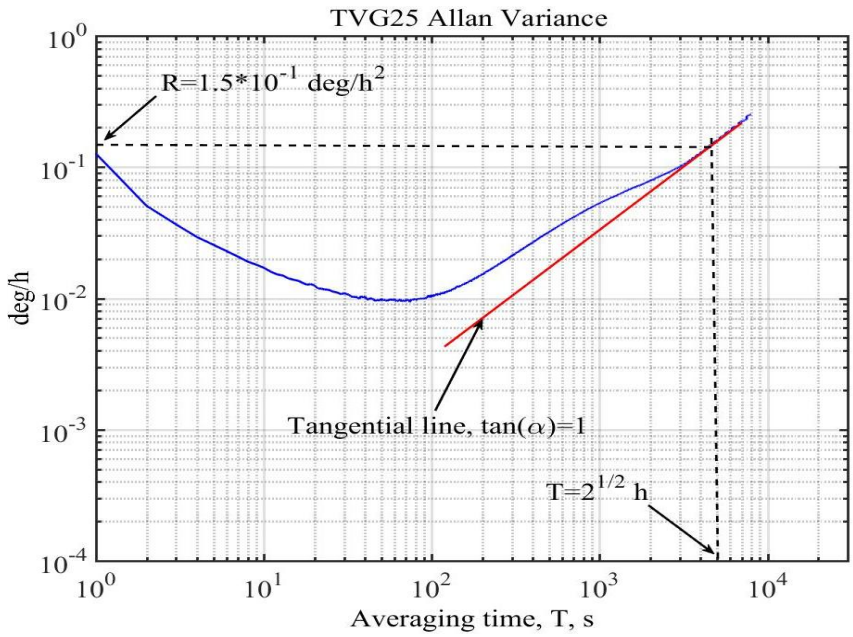

Fig. 2.5.7. Determination of rate ramp for TVG-25

Using appropriate mathematical models, error parameters are estimated. Here are some examples:

- KVB: The variance of the KVB σ^2KV^2 can be estimated as the variance of the AK at $\tau = 1$ s.
- RVB: The variance of the RVB σ^2RV^2 can be estimated as the variance of the AC at $\tau = 100$ s.
- Shear instability: the shear instability variance σ^2A^2 can be estimated as the variance of the AC at $\tau = 10000$ s.

2.6. Examples of the application of Allan's analysis of variation for low-grade and high-grade gyroscopes

Low-grade gyroscopes are inertial sensors used to measure angular velocity. Their characteristics:

- Low price: The price of low-grade gyroscopes can be 10-100 times less than that of high-grade gyroscopes.
- Small size and weight: This makes low-grade gyroscopes easy to integrate into compact devices.
- Low power consumption: This makes them ideal for portable devices.
- Low accuracy: Low-grade gyroscopes have higher noise and error levels, making them unsuitable for precise angle determination.
- Limited measurement range: Low-grade gyroscopes have a smaller measurement range than high-grade gyroscopes.
- Sensitivity to vibrations: Low-grade gyroscopes are more sensitive to vibrations, which can lead to measurement errors [28].

Types of low-grade gyroscopes:

Mechanical gyroscopes: These gyros use a rotating disc or pendulum to measure angular velocity. Piezoelectric gyroscopes: These gyroscopes use piezoelectric materials to measure the strain that occurs during rotation. MEMS gyroscopes: These gyroscopes are made using microelectromechanical systems (MEMS) and are the most common type of low-grade gyros [29].

High-grade gyroscopes are inertial sensors used to measure angular velocity with high accuracy. Their characteristics:

- High accuracy: High-grade gyroscopes have significantly less noise and error than low-grade gyroscopes.
- Wide measurement range: High-grade gyros can measure angular velocity over a wider range than low-grade gyros.
- Resistance to vibrations: High-grade gyroscopes are less sensitive to vibrations than low-grade gyroscopes.
- High price: High-grade gyros are significantly more expensive than low-grade gyros [30].

Types of high-grade gyroscopes:

Ring laser gyroscope (RLG): These gyros use the properties of laser radiation in a closed loop to measure angular velocity. Fiber optic gyroscope (FOG): These gyros use the properties of light in an optical fiber to measure angular velocity. Quantum gyroscopes: These gyroscopes use the principles of quantum mechanics to measure angular velocity. Ring laser gyros (RLG) and fiber optic gyros (FOG) are the two most common types of high-grade gyros [31].

Examples of the application of Allan's Analysis of Variation (AAV) to high- and low-grade gyroscopes:

- Calibration: VAA can be used to determine the error parameters of gyroscopes. These parameters can then be used to compensate for errors and improve the accuracy of angular velocity measurements.
- Condition monitoring: VAA can be used to monitor the condition of gyroscopes over their lifetime. This can help detect deterioration in gyro performance before it leads to failure.
- Training: The VAA can be used to teach the basics of inertial navigation and error theory.

Low-grade gyroscopes:

- Production quality control: Checking batches of gyroscopes for compliance with the characteristics declared by the manufacturer. Determination of limits for the parameters of the Allan's dispersion curve (AK). Identification and correction of problems in the production process.
- Diagnosis of malfunctions: Detection of wear or damage to the gyroscopes. Determine the type of fault. Decide whether to repair or replace the gyro.
- Compare characteristics: Select the gyroscope with the best price/performance ratio.
- Evaluate accuracy and reliability: Determine if a gyro is suitable for a particular application.

High-grade gyroscopes:

- Evaluate accuracy: Evaluate the accuracy of gyroscopes in the lab. Ensure that the product meets the declared specifications.
- Fault diagnosis: Detect wear or damage to gyroscopes.
- Scientific research: Study the characteristics of gyroscopes. Develop new methods and algorithms for inertial navigation.

The main differences are that high-grade gyroscopes are more accurate, meaning that VAA can be used to detect smaller errors and noise. They also have a wider measurement range, meaning that VAA can be used over a wider range of angular velocities. Resistance to vibrations VAA is less sensitive to vibrations, which gives more accurate results [32].

The main differences between low-grade and high-grade gyroscopes are that they are less accurate, and the VAA can only be used to determine larger errors and noise. Narrow measurement range, VAA can only be used in a narrow range of angular velocities. Sensitivity to vibrations, VAA is more sensitive to vibrations, which can lead to errors in the results.

In general, VAA is a more powerful tool for analyzing high-grade gyros than low-grade gyros.

SECTION 3
APPLICATION OF THE ALLAN VARIATION ANALYSIS TO THE HIGH-GRADE HRG

3.1. Allan variance computation algorithm

The Allan variance computation algorithm is a crucial tool in evaluating the performance of high-grade gyroscopes. By analyzing the characteristics of errors exhibited by gyroscopic systems, this algorithm provides insights into their stability, accuracy, and reliability. It aids in quantifying various error components such as quantization white noise, angle random walk, correlated noise, bias instability, rate random walk, and rate ramp, which are fundamental in understanding the overall performance of gyroscopes.

Having this algorithm is essential because it allows engineers and researchers to:

1. **Assess Performance:** The algorithm enables the assessment of gyroscopic system performance by quantifying different error sources. This assessment is vital in determining the suitability of gyroscopes for specific applications where high precision and stability are required.
2. **Optimize Calibration:** By understanding the error characteristics, the algorithm helps in optimizing calibration procedures. It allows for fine-tuning of gyroscopic systems to achieve optimal accuracy and minimize errors.
3. **Predict Behavior:** With the Allan variance analysis, it becomes possible to predict the behavior of gyroscopic systems over time. This predictive capability is valuable for long-term applications where consistent performance is crucial.

4. **Compare Different Systems:** The algorithm facilitates comparisons between different gyroscopic systems based on their Allan variance curves. This comparative analysis aids in selecting the most suitable gyroscopes for specific operational requirements.

The process of calculating the Allan variance (AV) to characterize the gyroscope output data will be discussed in more detail in this algorithm.

1. Dividing data into bins depending on the averaging time interval (τ) as displayed on Fig. 3.1.1-3.1.3:

- **Selecting a time interval:** The first step is to select the averaging time interval, denoted as τ. This can be, for example, 1 second, 10 seconds, or any other appropriate interval depending on the characteristics of the device and the needs of the study.
- **Formation of bins:** Next, the long time series is divided into bins, where each bin contains data averaged over a selected time interval τ.

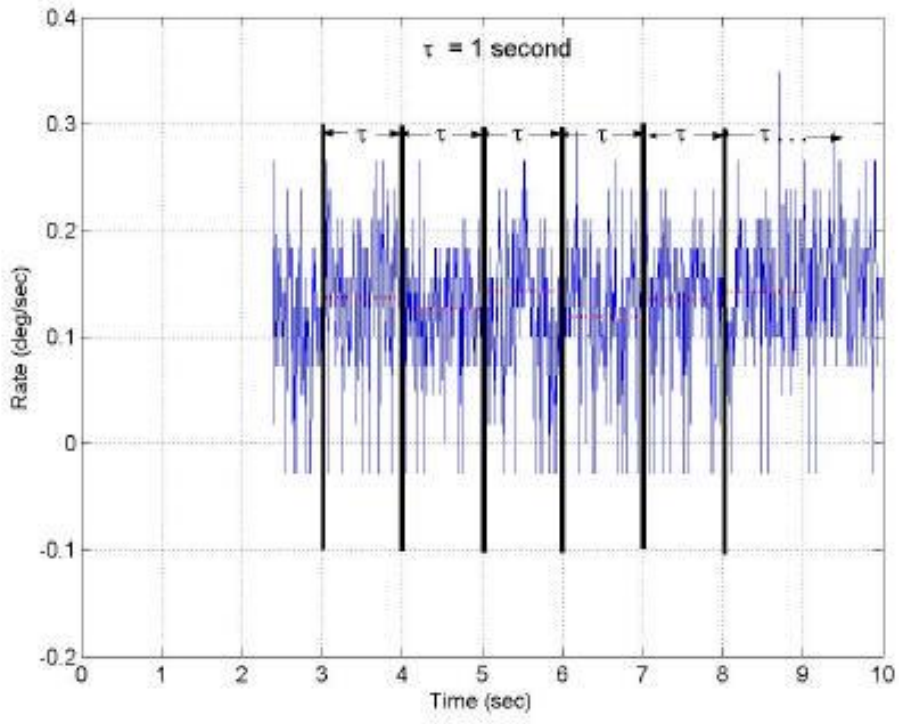

Fig. 3.1.1. Data divided into bins of 1 second length

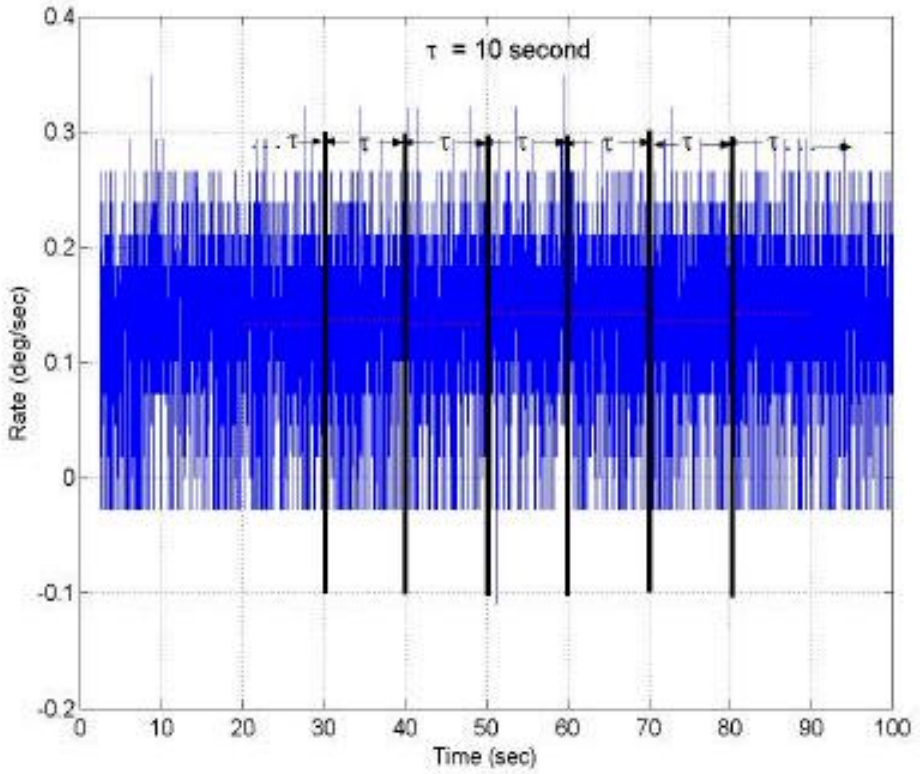

Fig. 3.1.2. Data divided into bins of 10 second length

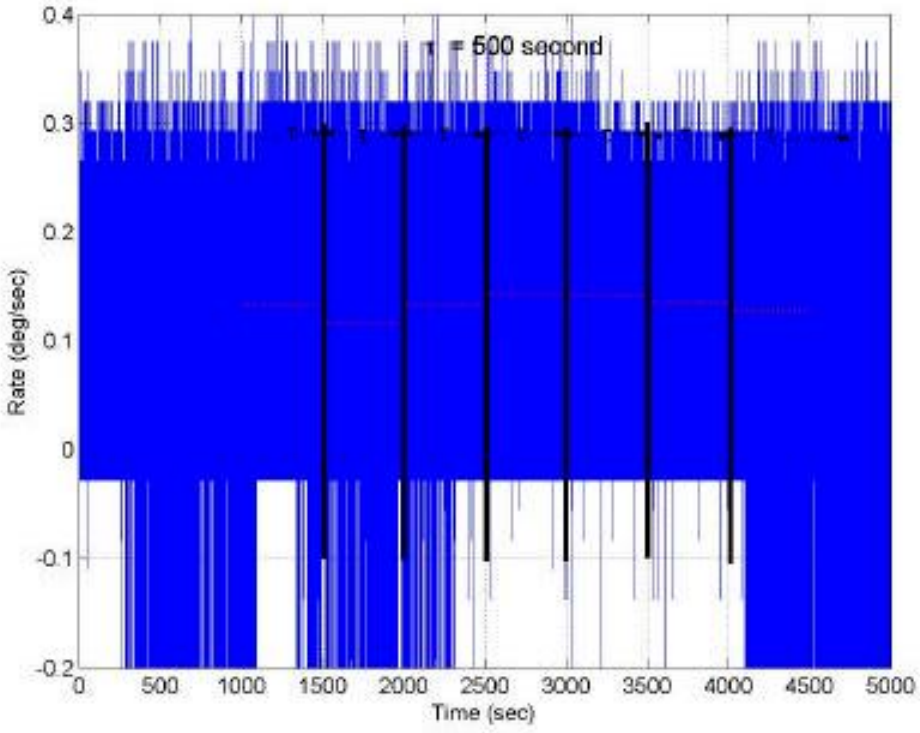

Fig. 3.1.3. Data divided into bins of 500 second length

2. **Calculating the Average Value for Each Bin:**
    - After splitting into bins, you calculate the average gyro value for each bin. This is done by calculating the arithmetic mean of all the data in each bin.
3. **Calculating the Square of the Differences:**
    - You then calculate the square of the difference between the mean values for each pair of adjacent bins. This means that you take the square of the difference between the mean values of the known gyro parameters in one bin and its predecessor in the other bin.
4. **Average of Squared Differences:**
    - Finally, you calculate the average of all the squares of the differences you obtained in the previous step. This helps you to find the average of the squared deviations between the mean values in the neighboring bins.

The equation for AV is defined as follows:

$$AV = \frac{1}{2(N-1)} \sum_{k=1}^{N} (a(\tau)_i - a(\tau)_{i-1})^2 \,.\#(3.1)$$

where N is the number of bins of gyro data;

$a(\tau)_i$ represents the average over the ith bin of duration τ.

It's crucial to note that not all values of τ are valid for use in equation (3.1). A general rule is to use at least nine data values when calculating averages for AV.

$$\Delta t = \frac{total\ duration\ of\ dataset}{N} .\#(3.2)$$

Equation (3.2) sets a lower limit for τ based on this requirement, considering the temporal spacing Δt between gyro data values.

$$duration \geq 9 \times \Delta t .\#(3.3)$$

Equation (3.3) gives an upper limit for τ based on the total duration of the dataset (duration) and the number of bins (N), ensuring at least nine bins of duration τ

are present in the dataset. A typical valid range for τ values is from 0.1 seconds to over 1000 seconds.

The bias stability, a common performance metric for gyros, is derived from the AV curve. Specifically, it corresponds to the minimum value on the Allan Deviation (AD) curve, where AD is the square root of the AV.

Once the calculation is complete, the AVAR results can be plotted against τ. Fig. 3.1.4 illustrates the outcomes for this dataset alongside the computation error. To enhance clarity, the AVAR data is graphed on a logarithmic scale.

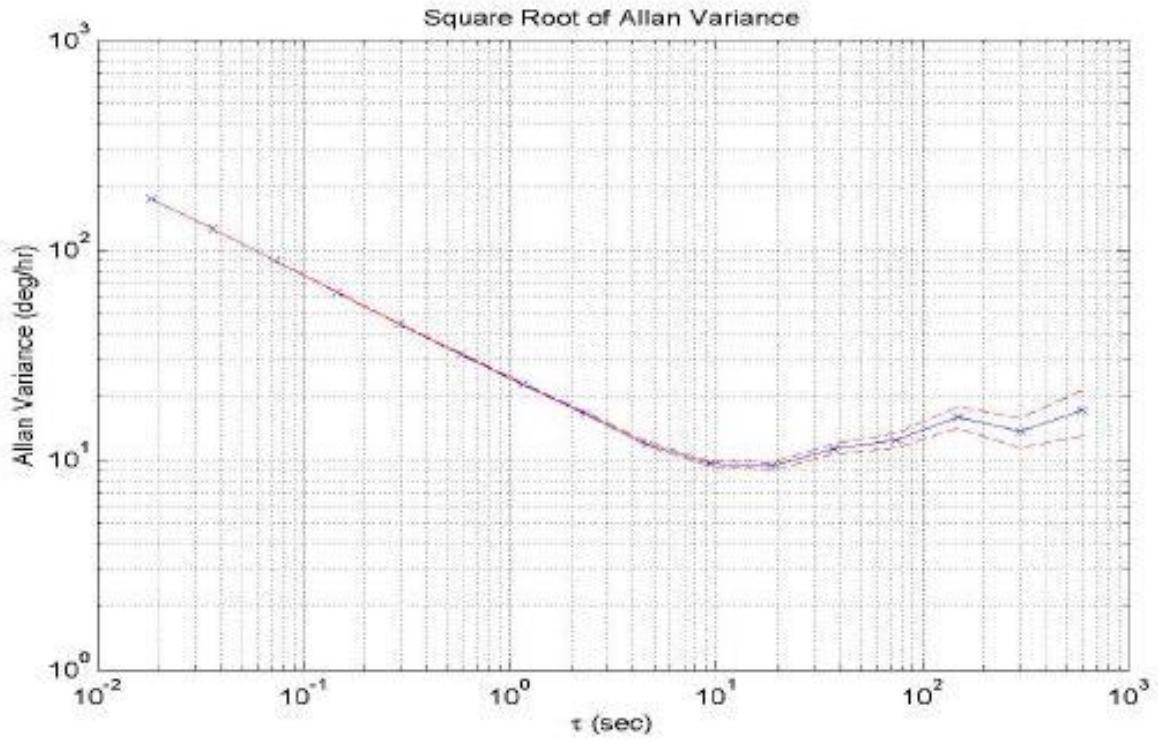

Fig. 3.1.4. The Allan Variance result for the rate sensor data. (The red lines show the error limits in the calculation)

3.2. The high-grade HRG noise analysis

Hemispherical resonator gyroscope (HRG) produced by Sagem (Safran group, France) was presented in fig. 1.5.1 in section 1. Temperature profile of HRG testing in the temperature range [-15 +45] ℃ is depicted in Fig. 3.2.1. The HRG output signal in this temperature range is presented in Fig. 3.2.2.

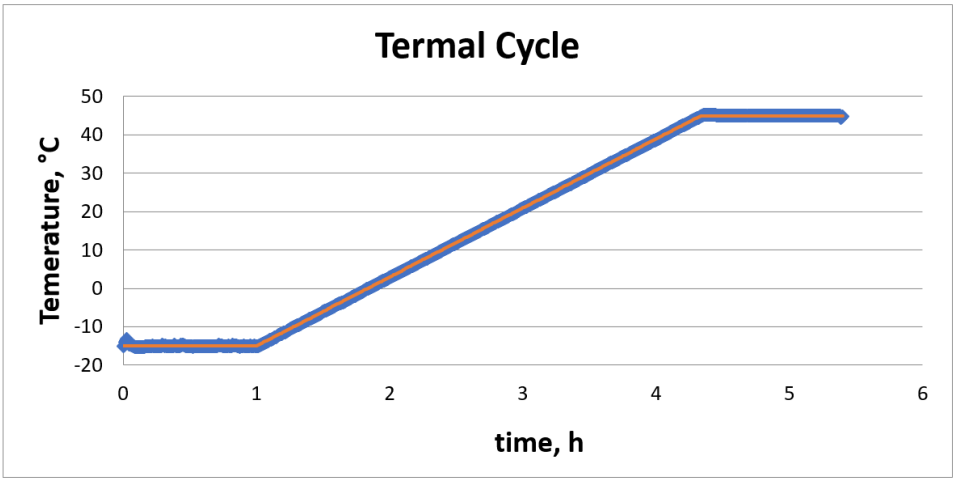

Fig. 3.2.1. Thermal cycle for Sagem HRG

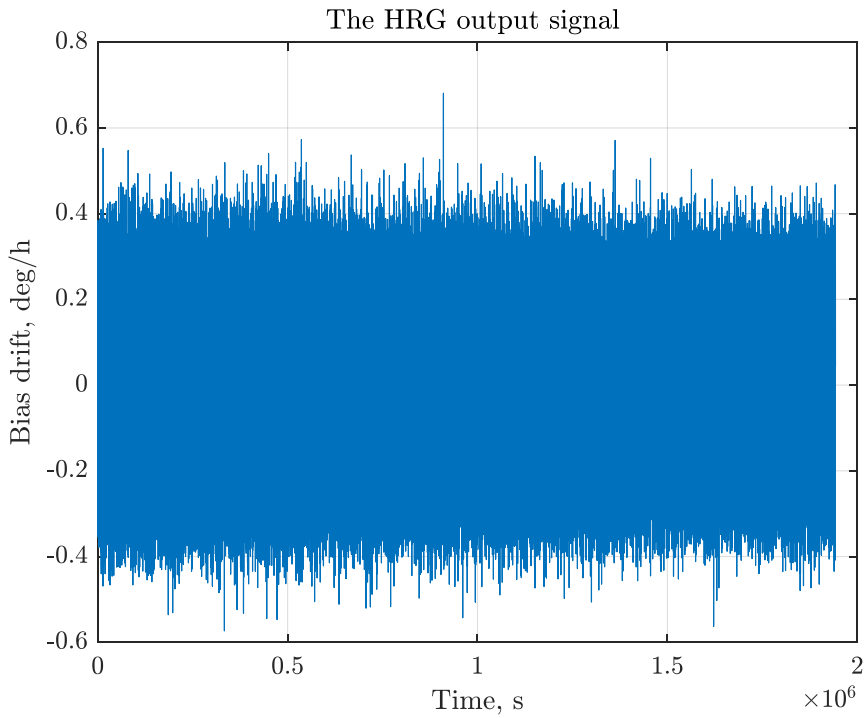

Fig. 3.2.2. The HRG output signal

As a practical example, let's consider the square root of Allan variance of the high-grade HRG in Fig. 3.2.3.

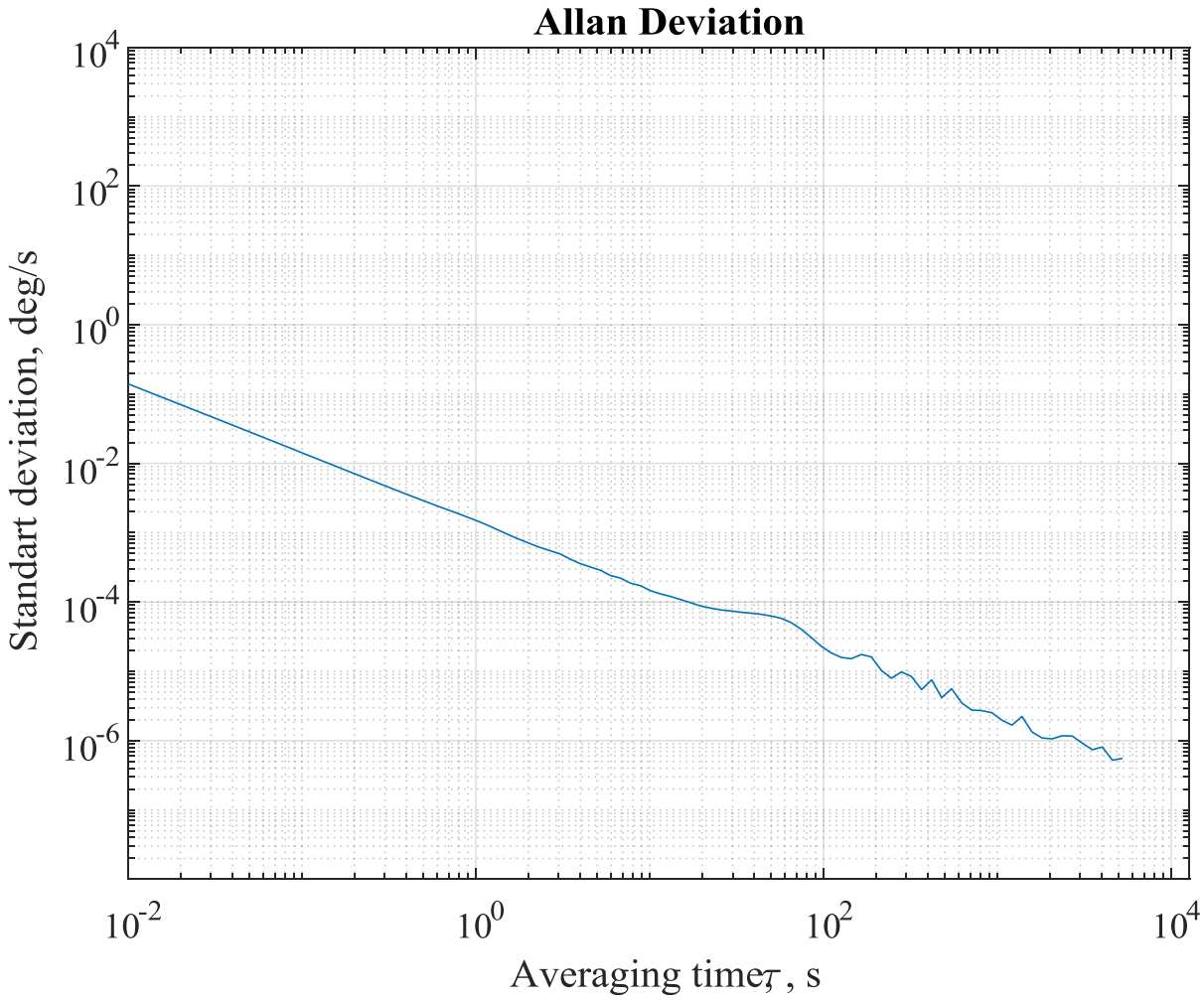

Fig. 3.2.3. Allan standard deviation

Correlation function $C_M(t)$ of the exponentially correlated noise parameters τ_c and M determination example, using another gyro (non-vibrating one) root square (standard deviation) of Allan variance curve is presented below.

Correlation time τ_c for this noise is determined, in correspondence with (2.17), by the ratio $\tau/\tau_c = 1.89$, where τ is an averaging time at which the maximum of a convex part of the curve is reached. This maximum, as can be seen from fig. 3.2.4, is reached at $\tau \approx 63$ s, so $\tau_c \approx 63/1.89 \approx 33.3s \approx 0.0093$ h.

The maximum of this convex part is 0.000058 deg/h = 0.21 (see Fig. 3.2.4), so for the M coefficient, in correspondence with (2.17), the following value can be obtained:

$$0.437M\sqrt{\tau_c} = 0.000058 \text{ deg/s} \approx 0.21 \text{ deg/h} \rightarrow$$

$$M = \frac{0.21}{0.437\sqrt{0.0093}} \approx 0.096 \text{ deg/h}^{3/2}.$$

Thus, there is exponentially correlated (Markov) noise in the output of this gyro with the following correlation function:

$$C_M(\tau) = \frac{0.0014}{\sqrt{3}} e^{\tau/33.3} = 0.000808e^{\tau/33.3} \text{ deg/h}^{3/2} .$$

where the dimension of τ is seconds.

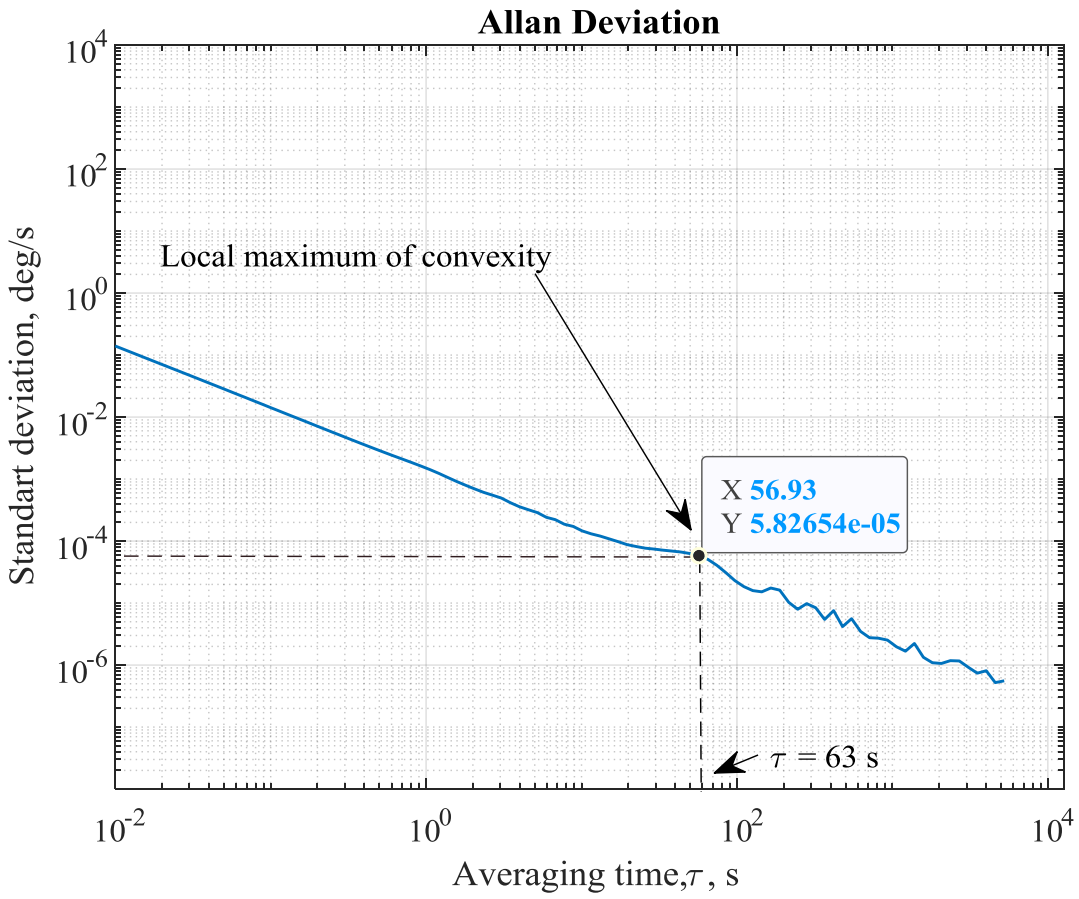

Fig. 3.2.4. Local maximum of convexity in the Allan curve

Sinusoidal noise parameters determination, using HRG gyro output signal, Allan curve of which is presented in Fig. 3.2.5.

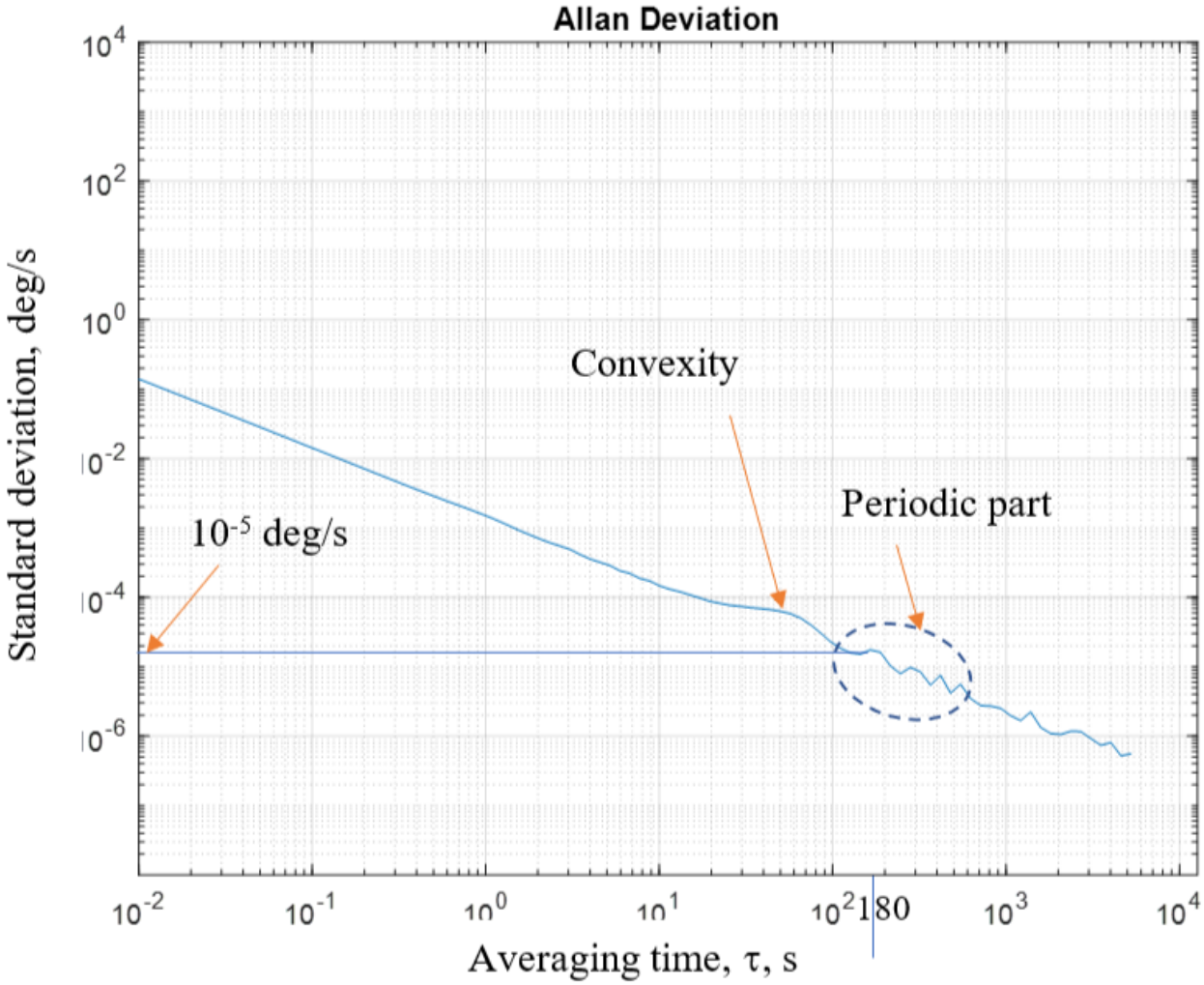

Fig. 3.2.5. Periodic part in the Allan curve

In correspondence with (2.19), the sinusoidal noise frequency is

$$f_0 = 0.371/\tau_s.$$

As can be determined from fig. 3, τ_s is $\tau_s = 180$ s, hence

$$f_0 = 0.371/180 = 0.002 \text{ Hz}.$$

Amplitude of the sinusoidal noise Ω_0 is determined from (2.19) as follows:

$$\sigma_\Omega(\tau_s) = 0.725\Omega_0; \sigma_\Omega(\tau_s) = 0.725 * 10^{-5} \text{ deg/s} = 0.0261 \text{ deg/h}.$$

Thus, sinusoidal noise in HRG gyro, as follows from (2.16), can be represented to be:

$$\sigma_\Omega(\tau) = 0.0261 \frac{sin^2 2\pi f_0 \tau}{\pi f_0 \tau} \text{ deg/h}; \; f_0 = 0.002 \text{ Hz}.$$

Angle random walk parameter determination, using HRG gyro output signal, Allan curve of which is presented in Fig. 3.2.6.

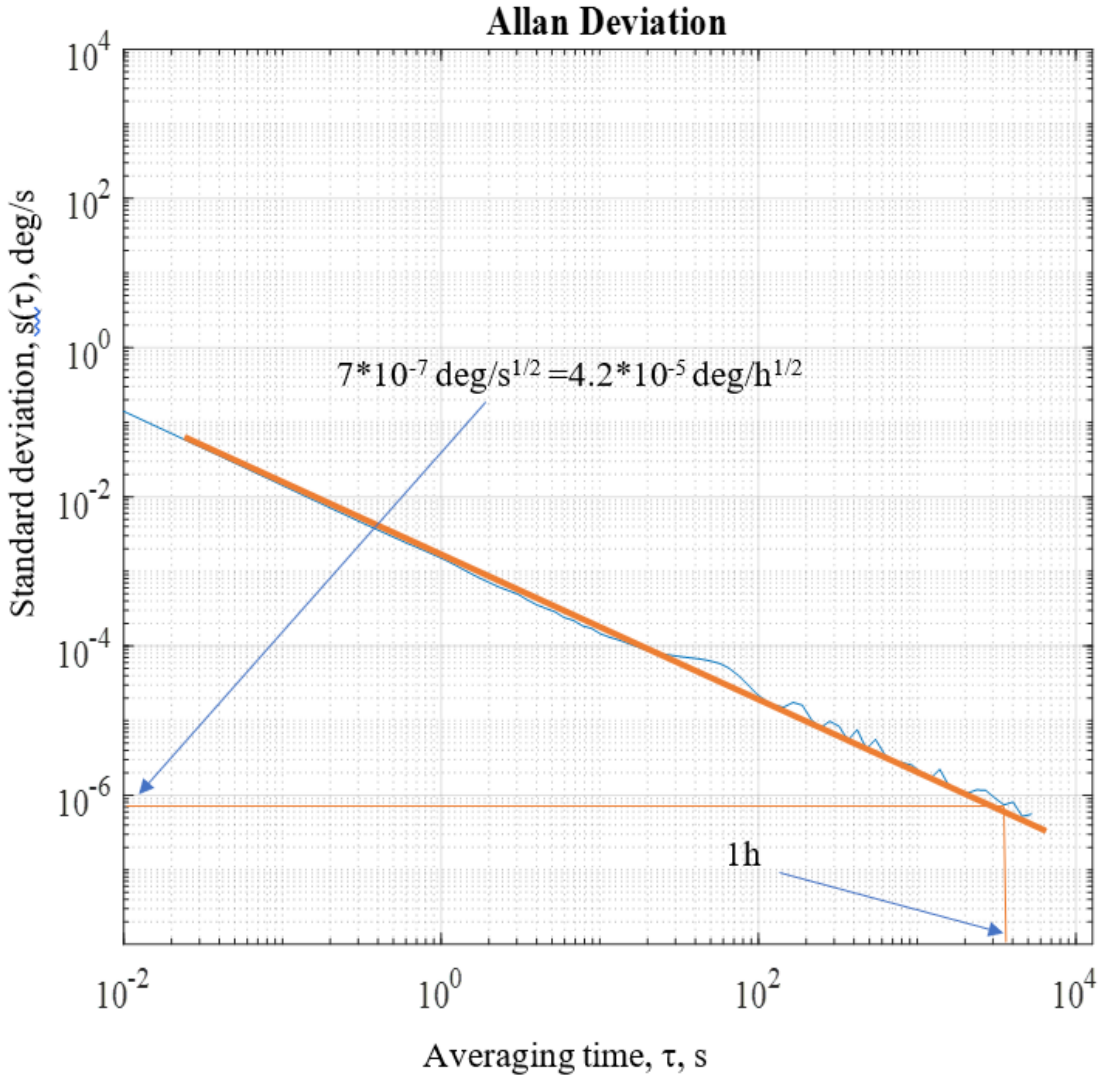

Fig. 3.2.6. Calculation of an angle random walk by the Allan curve

The value of N was determined by finding the point of intersection of the tangent line with a slope of -0.5 and the vertical line starting at time *T = 1* hour on the Allan Curve.

This point of intersection indicates the value of N, which in this case is

$$\mathrm{N} = 4.2 * 10^{-5}\ \mathrm{deg/h^{1/2}}\ ,$$

reflecting the noise level or measurement variations in the system.

3.3. Interpretation of the results

Based on the calculations and analysis of the Allan variance curve for the gyroscope, several conclusions can be drawn below.

Exponentially Correlated Noise (Markov Noise): The calculations revealed the presence of exponentially correlated noise in the gyroscope. This type of noise, known as Markov noise, is characterized by the fact that the noise values at the current time step depend on previous noise values. This may be caused by internal processes in the gyroscope or a known systematic error in its operation. The correlation function $C_{M(\tau)} = 0.000808e^{\tau/33.3}$ shows how the correlation between different noise values decreases over time. Understanding this noise is important in designing and improving gyroscopes to reduce the impact of noise on their accuracy and stability.

Sinusoidal Noise: The detection of sinusoidal noise in the gyroscope indicates periodic oscillations in its output data. This may be due to external influences on the gyroscope or internal mechanical or electrical processes. The calculations showed the frequency of this noise $f_0 = 0.002$ Hz and its amplitude $\Omega_0 = 0.0261$ deg/hour. Understanding this noise is important for compensating for its impact on

measurements and improving the accuracy of the gyroscope in various environmental conditions.

The limitation in studying the instability of the zero offset lies in some limitations arising from data collection and analysis. First of all, in order to detect the minimum of the Allan curve and further analyze the growth of the zero-displacement instability, a sufficiently long averaging time (τ) must be used, which ideally should exceed 10,000 seconds. However, in real-world conditions, especially when measuring with highly sensitive gyroscopes, such an averaging time may be difficult or even impossible to achieve due to limited measurement duration or technical limitations in data processing.

Detection of noise components: Despite the difficulties in analyzing the zero-displacement instability, the study successfully detected important noise components such as exponentially correlated Markov noise and sinusoidal noise. These discoveries are important for understanding gyroscope behavior in different conditions and environments.

3.4. Conclusion

In this part of the section, I performed calculations using the Allan analysis method for a high-quality gyroscope using the Allan variance calculation algorithm. These calculations provided important data on the characteristics of noise and measurement errors, which are critical for assessing the accuracy and reliability of the gyroscope. In particular, the parameters of exponentially correlated noise (Markov noise), sinusoidal noise, and random error parameters were determined.

These calculations allow us to understand which specific noises affect the gyroscope's performance, what are the characteristics of these noises, and how they change over time. This analysis is key to improving gyro performance, correcting errors, and increasing accuracy. Some of the noise detected may be standard for this

type of gyro, but others may indicate problems with the gyro itself or its sensors. Therefore, it is important to continue research in this area to improve technology and increase the accuracy and reliability of inertial measurement systems.

Furthermore, the Allan variance method is especially useful for distinguishing between different types of noise and understanding their impact on long-term stability. By analyzing the Allan variance plot, one can identify various noise processes such as white noise, random walk, and flicker noise, and assess their respective contributions to the overall measurement uncertainty. This information is crucial for developing noise reduction strategies and improving the design of gyroscopic systems.

The results of these calculations also provide valuable insights into the behavior of the gyroscope under different operating conditions. For example, understanding the temporal characteristics of noise can help in designing more effective filtering and compensation techniques. This is particularly important for applications requiring high precision, such as navigation systems in aerospace and marine environments, where even small errors can accumulate over time and lead to significant deviations.

In addition, the knowledge gained from Allan variance analysis can be used to optimize the gyroscope's electronic and mechanical components. By identifying the sources of noise and their characteristics, engineers can make informed decisions about material selection, sensor design, and signal processing algorithms. This can lead to the development of gyroscopes with enhanced performance, greater reliability, and longer operational lifetimes.

CONCLUSION

In the bachelor's thesis, the estimation of the bias components of modern high-precision gyroscopes was performed using the Allan variance. The main types of high-precision gyroscopes, such as ring laser resonator gyroscopes (RLG), fiber optic gyroscopes (FOG), and quartz resonator gyroscopes (HRG), are described, including their manufacturers, characteristics, and applications in inertial measurement systems.

The Allan analysis method is also considered, which allows to present models of random errors determined by the Allan dispersion curve, such as quantum white noise, random angular motion error, correlated noise, periodic noise, bias instability, angular random walk, and rate ramp. A methodology for estimating these error parameters is presented.

The application of Allan's analysis to the HRG high-precision gyroscopes provided important data on the noise characteristics and measurement errors, which is critical for assessing the accuracy and reliability of gyroscopes. The research results can be used to improve gyroscope manufacturing technologies and increase their performance and measurement accuracy in the future.

REFERENCES

1. https://science.howstuffworks.com/gyroscope.htm [Electronic source]
2. https://www.britannica.com/technology/gyroscope [Electronic source]
3. https://aerospace.honeywell.com/us/en/about-us/blogs/how-does-ring-laser-gyroscope-work [Electronic source]
4. https://www.advancednavigation.com/glossary/ring-laser-gyroscope [Electronic source]
5. https://w.wiki/_sxaJ [Electronic source]
6. https://jak.koshachek.com/articles/princip-roboti-lazernogo-giroskopa.html [Electronic source]
7. http://www.mh-elec.com/photo-x.php?id=186 [Electronic source]
8. https://uk.wikipedia.org/wiki/%D0%9B%D0%B0%D0%B7%D0%B5%D1%80%D0%BD%D0%B8%D0%B9_%D0%B3%D1%96%D1%80%D0%BE%D1%81%D0%BA%D0%BE%D0%BF [Electronic source]
9. https://jrnl.nau.edu.ua/index.php/ESU/article/view/887/869 [Electronic source]
10. https://www.canalgeomatics.com/knowledgebase/how-do-fiber-optic-gyros-work/ [Electronic source]
11. https://www.coherent.com/news/glossary/fiber-optic-gyroscope [Electronic source]
12. https://spaceequipment.airbusdefenceandspace.com/avionics/fiber-optic-gyroscopes/astrix-1000/ [Electronic source]
13. https://www.collinsaerospace.com/what-we-do/industries/military-and-defense/navigation/weapons-products/guidance-navigation-control/inertial-navigation-systems [Electronic source]
14. https://www.gemrad.com/fiber-optic-gyrocompass/ [Electronic source]
15. https://www.tronics.tdk.com/inertial-sensors/high-performance-mems-inertial-sensors/gypro-high-performance-mems-gyroscopes/ [Electronic source]
16. https://device.report/m/ca9f3f64f24d8ac5b403f1336f5226a77d44b9e3f7945459c61ab5b818051162.pdf
17. https://www.electricity-magnetism.org/hemispherical-resonator-gyroscope/ [Electronic source]
18. https://en.wikipedia.org/wiki/Hemispherical_resonator_gyroscope [Electronic source]
19. https://www.electricity-magnetism.org/hemispherical-resonator-gyroscope/ [Electronic source]
20. https://en.m.wikipedia.org/wiki/Inertial_navigation_system [Electronic source]

21. https://en.m.wikipedia.org/wiki/Attitude_and_heading_reference_system [Electronic source]
22. The state and prospects of the development of vibration gyroscopy in Ukraine and in the world Valerii Chikovani, Sergii Golovach [p. 21-23]
23. https://www.allaboutcircuits.com/technical-articles/intro-to-allan-variance-analysis-non-overlapping-and-overlapping-allan-variance/ [Electronic source]
24. https://home.engineering.iastate.edu/~shermanp/AERE432/lectures/Rate%20Gyros/Allan%20variance.pdf [Electronic source]
25. A. Papoulis, Probability, Random Variables, and Stochastic Process, 3rd ed. New York: McGraw-Hill, 1991.
26. Analysis and Modeling of Inertial Sensors Using Allan Variance Naser El-Sheimy, Haiying Hou, and Xiaoji Niu
27. D-TACQ Solutions Ltd, Copyright © 2019 Allan Deviation Made Simple May 2023 Mark HoseyMark Hosey
28. https://www.analog.com/en/resources/technical-articles/gyro-mechanical-performance.html [Electronic source]
29. Two types of micromachined vibratory gyroscopes A.M. Shkel, C. Acar, C. Painter
30. https://www.vectornav.com/resources/inertial-navigation-primer/theory-of-operation/theory-gyros [Electronic source]
31. https://park.zapisi.cx.ua/ukraincyam/yaki-buvayut-giroskopi-vidi-princip-roboti-zastosuvannya.html [Electronic source]
32. Roberts C.A., Morgan P., Rizos C. Allan variance applied to time series baseline results for GPSbased deformation monitoring applications. In: 2nd Symposium on Geodesy for Geotechnical and Structural Applications, Berlin, Germany, 21-24 May, 2002, 299-311.